NASA Surface meteorology and Solar Energy: Methodology

12/16/04

1. INTRODUCTION

Historically, climatological profiles of insolation and meteorology parameters calculated from ground measurements have been used for determining the viability of Renewable Energy Technology (RET) projects. These climatological profiles are used for designing systems that have low failure rates. Although ground measurement data has been used successfully in the past for implementing RETs, there are inherent problems in using them for resource assessment. Ground measurement stations are located throughout the world, but they are situated mainly in populated regions. In remote areas (where many RETs are implemented) measurement stations are limited. Also, at any particular station, data recording can be sporadic leading to incomplete climatological profiles; and, data inconsistencies can occur within a station and from one station to another. In contrast to ground measurements, the SSE data set is a continuous and consistent 10-year global climatology of insolation and meteorology data on a 1^o x 1^o grid system. Although the SSE data within a particular grid cell are not necessarily representative of a particular microclimate, or point, within the cell, the data are considered to be the average over the entire area of the cell. For this reason, **the SSE data set is not intended to replace quality ground measurement data**. Its purpose is to fill the gap where ground measurements are missing, and to augment areas where ground measurements do exist. In utilizing the SSE data set, an estimate of the renewable energy resource potential can be determined for any location on the globe. That estimate may be accurate enough for preliminary feasibility studies of new renewable energy projects. In addition, SSE provides year-to-year variability in terms of 10-year maximums and minimums for a number of parameters. In some situations, **variability data may be more valuable than precise average values**.

The **purpose** of this document is to provide information describing how various parameters were obtained, their limitations, and estimated accuracies based on information available to NASA at the time of this manuscript. The **intent** is to provide **maps** and **accuracy charts** such that a user may make decisions concerning suitability of the SSE data for his or her project in a particular region of the globe. **Equations** and **assumptions** are provided to further assist in understanding limitations of the data and improve use by the college and university community. In general, meteorology and solar insolation were obtained from the **NASA Earth Science Enterprise (ESE) program's satellite and reanalysis research data**. Additional parameters were estimated and validated based on **recommendations from partners in the energy industry**.

Researchers from several organizations in various locations developed the methods used. The methods have been applied to other locations that **may** or **may not** have the same climate characteristics as the original development/verification region. This document will describe methods, accuracies, and limitations relative to various climate regions over the globe. We follow the general style of RETScreen documentation, but go slightly further in graphics detail in order to define those regions over the globe where methodologies are inconsistent or new information is needed.

2. CONTENTS

1. INTRODUCTION

2. CONTENTS

3. CLIMATE REGIONS

4. HORIZONTAL SURFACE INSOLATION

5. HORIZONTAL DIFFUSE AND SOLAR BEAM DIRECT NORMAL RADIATION (DNR)

5.1 Monthly Horizontal Diffuse Methods

5.1.1 Erbs et al. Method

5.1.2 Extended Page Method

5.2 Comparison of Diffuse Methods

5.3 Monthly DNR Methods

5.3.1 RETScreen-type Method

5.3.2 Extended Page/Empirical Staylor Method

5.4 Comparison of DNR Methods

6. MONTHLY TILTED SURFACE RADIATION

6.1 Monthly Tilted Surface Methods

6.1.1 RETScreen Isotropic Method

6.1.2 Perez Non-Isotropic/Extended Page Horizontal Diffuse Method

6.1.3 Perez Non-Isotropic/Erbs et al. Horizontal Diffuse Method

6.2 Comparison of Tilted Surface Methods

7. WIND SPEED PARAMETERS

8. TEMPERATURE, PRESSURE, AND HUMIDITY PARAMETERS

8.1 Near-surface Air Temperature

8.2 Surface Air Pressure

8.3 Relative Humidity

8.4 Precipitation

9. REFERENCES

3. CLIMATE REGIONS

NASA is sensitive to the fact that surface radiation methodologies developed and verified in one region of the globe may not produce reasonable results in other climate regions. Issues are (1) predominant cloud types may be different (thicker or thinner), (2) atmospheric aerosols may be more or less absorbing, (3) surfaces may have large differences in albedo, and (4) seasonal wind patterns may transport significant pollutants either in or out of the region. Ignoring regional differences has resulted in surface insolation bias errors as large as 35% (Ref. [1]).

The climate classification of Smith et al. (Ref. [2]) is assumed for this analysis. Figure 1 shows a map of the climate regions as well as criteria for each region. The classification is based on the amounts of net solar and thermal infrared radiation absorbed into the Earth's surface below clouds, aerosols, water vapor, ozone, etc. in the atmosphere. Factors most influential on shortwave (SW) surface-absorbed energy are surface albedo (Fig. 2), daylight cloud amount (Fig. 3), and insolation clearness index (Fig. 4). The monthly average clearness index, k, is defined as the monthly average horizontal insolation impinging on the Earth's surface, H, divided by the monthly average incoming top-of-atmosphere horizontal insolation, H_o. The parameter combines total atmospheric transmissivity losses from cloud amount, thickness, and absorption; aerosol absorption and scattering; as well as molecular, ozone, and water vapor absorption. Clearness index is used in a number of energy industry equipment design procedures.

4. HORIZONTAL SURFACE INSOLATION

Release 5 SSE horizontal surface insolation values, H, are different than those provided in Release 4 SSE. For Release 5, insolation values were calculated using the Pinker and Laszlo algorithm (version 2.1) as processed under the NASA/Global Energy and Water Cycle Experiment (GEWEX) Surface Radiation Budget (SRB) project and represents Release 2 solar radiation from this project. Upgrades from the original Pinker and Laszlo algorithm (Ref. [3]) to version 2.1 include the treatment of water vapor, filling strategies and spectral albedo information.

Major inputs to the insolation calculations were obtained from the World Climate Research Program's International Satellite and Cloud Climatology Program (ISCCP) sponsored by NASA (Ref. [4]). Version DX 8-km radiance and cloud were used. Water vapor was taken from the NASA Data Assimilation Office's Version 1 Goddard Earth Observation System (GEOS-1) data for each 2^o x 2.5^o latitude/longitude cell over the globe for the period July 1983 through June 1993 on a 3-hourly basis (Ref. [5]). Ozone is taken from the Total Ozone Mapping Spectrometer (TOMS) for the 1983 through 1993 period. Depending on the cell size of the source, all data are converted and presented on a true 1^o x 1^o grid using various spatial averaging, interpolation, or replication techniques.

Aerosol and cloud optical depths are used as tuning parameters in the Pinker and Laszlo algorithm. Any difference between ISCCP clear-sky composite radiance and instantaneous radiance is ascribed to aerosol in the clear fraction of the grid box, and to cloud optical depth in the cloudy fraction. The resulting aerosol field in particular is not representative of a realistic aerosol field. The cloud optical depth returned by the algorithm agrees fairly well with the ISCCP-derived optical depth, except over ice.

Figure 5 provides maps of 10-year average insolation for both January and July. Patterns appear similar to those of daylight cloud amount in Fig. 3, but are modified significantly by other cloud, atmospheric, and seasonal parameters as noted above.

The 10-year data period contained 3.5 El Nino years, 2 La Nina years, and 4.5 "near-average" years (Ref. [6]). Many different types of meteorological events that created variations in clouds, water vapor, ozone, winds, etc. cause year-to-year variations in the SSE data. Estimated RMS uncertainties of monthly average Release 5 SSE using operational WRDC data are generally in the 16% range and bias is much less than 1%.

Release 5 has also been tested against research-quality Baseline Surface Radiation Network (BSRN) data for the 1992 through 1995 period. Figure 6 shows insolation uncertainties for various data time spans. Three-hourly incremental data (upper left chart) has the most noise (RMS = 46%, Bias = -3.2%) as would be expected because of satellite navigation uncertainties and cell-size issues. If 3-hourly values are averaged over the month on an hourly basis, the resulting monthly average diurnal values (lower left chart) are more accurate (RMS = 21.7%, Bias = -3.5%). Daily values are obtained by averaging 3-hourly values over each day (upper right chart). Daily uncertainties are RMS = 22.6% and Bias = -2.5%. Monthly average uncertainties (lower right chart) are much more accurate (RMS = 13.5%, Bias = -2.5%).

5. HORIZONTAL DIFFUSE AND SOLAR BEAM DIRECT NORMAL RADIATION (DNR)

Estimates of horizontal diffuse, H_d, and direct normal radiation, DNR, are needed for hardware system design parameters such as solar panel tilt, solar concentrator size, daylighting, as well as agricultural and hydrology applications. There are no known methods of estimating these two parameters over the globe with proven accuracy. Two SSE industry partners recommended that NASA/SSE modify industry methods for application to monthly average satellite data as a possible approach. Preliminary design values might be obtained for regions over the globe where accurate ground site measurements are not available.

5.1 Monthly Horizontal Diffuse Methods

Historic studies (Refs. [7, 8], for example) as well as more recent research (Refs. [9 - 12]) indicate that ground site measurements of diffuse radiation are less accurate than once believed because of thermodynamic imbalances within some operational instruments if "shadow band" or "shadow disk" techniques are used. Important errors appear to be a function of cloud fraction suggesting daily changes in uncertainty. SSE may not be able to select a "best" method based on comparisons with historic ground site data. For this reason, several methods are used to estimate diffuse radiation.

5.1.1 Erbs et al. Method: This approach utilizes the simple method of Erbs et al. from Refs. [13, 14] as implemented by RETScreen (Ref. [15]). (See equations (5) and (6) in Chapter 4 at RETScreen site <http//www.retscreen.net/ang/12.php>.) The monthly diffuse to monthly horizontal insolation ratio is estimated from cubic polynomial equations in terms of insolation clearness index as follows:

$(H_d/H) = 1.391 - 3.569k + 4.189k^2 - 2.137k^3$ (1)

when the sunset hour angle, ω_s, for the "monthly average day" $\leq 81.4^o$. *

or

$(H_d/H) = 1.311 - 3.022k + 3.427k^2 - 1.821k^3$ (2)

when ω_s for the "monthly average day" $> 81.4^o$.

where:

$k = (H/H_o)$ is in the range $0.3 \leq k \leq 0.8$.

$\omega_s = \cos^{-1}[-\tan(\text{solar declination}) * \tan(\text{latitude})]$, (+ = west relative to solar noon). (3)

solar declination $= 23.45 * \sin[6.303 * \{(284 + n)/365\}]$ (4)

where:

n = day number of year, 1 = January 1.

Two different ranges of sunset hour angle are included to simulate seasonal effects.

An apparent strength of this method is that equations were derived from more-reliable pyroheliometer-measured DNR and horizontal insolation data from Texas, California, North Carolina, and Massachusetts instead of diffuse measurements. These sites are located in the temperate continental, subtropical land, and steppe/semi-arid climate regions shown in Fig. 1. Erbs et al. (ref. [13]) indicate that their method has a 4 to 6% monthly uncertainty relative to the original four test sites used to develop the polynomial equations. It also is in reasonable agreement (4 to 8% monthly uncertainties) with the original Page method (ref. [16]) for these particular test sites. It should be noted that that the Erbs et al. method has not yet been tested over all climate types because of the lack of combined pyroheliometer/insolation measurements in many regions of the globe.

Figure 4 suggests that regions with monthly average insolation k values outside $0.3 \leq k \leq 0.8$ tend to occur at latitudes beyond $\pm$ 50 degrees and at a few places in Asia. These "outside-Erbs" regions change in size and location if k is based on either maximum or minimum 10-year monthly average insolation values as shown in Figs. 7 and 8. Minimum insolation (and k) tends to increase the size of regions outside $0.3 \leq k$ and decreases the size of regions outside $k \leq 0.8$ as a result of increased clouds. The opposite happens for maximum insolation and k. **SSE does not provide Erbs et al. diffuse values in regions outside $0.3 \leq k \leq 0.8$ in this web site. Both DNR and tilted surface results are also omitted in the "outside Erbs" regions IF the method is dependent on Erbs et al. diffuse results.**

* The "monthly average day" is the day (in the month) whose declination is closest to the average declination for that month [S.A. Klein, Calculation of monthly average insolation on tilted surfaces, Solar Energy, 19, 325-329, 1977].

Month	Date in month	Declination	Month	Date in month	Declination
January	17	-20.9	July	17	21.2
February	16	-13.0	August	16	13.5
March	16	-2.4	September	15	2.2
April	15	9.4	October	15	-9.6
May	15	18.8	November	14	-18.9
June	11	23.1	December	10	-23.0

5.1.2 Extended Page Method: Based on results from both Vignola and McDaniels (Ref. [7]) and Brunger and Thevenard (Ref. [17]), the linear method of Page (Ref. [16]) was selected for testing. The diffuse to horizontal insolation ratio is estimated as:

$$H_d/H = [a + (b*k)] \quad (5)$$

where a and b for a particular cell are determined from comparison with a group of reference sites.

The original Page reference sites were augmented with newer diffuse and horizontal insolation site data from WRDC, NREL, CMDL, and the World Climate Research Program's Baseline Surface Radiation Network (BSRN). Figure 9 is a map showing the extended Page method reference sites, and Table 1 at the end of the text provides clearness index and a, b coefficient values derived for the reference sites. The extended Page method has 74 reference sites in 12 of the 13 climate regions shown in Fig. 1. Values in the table were obtained from both historic and recent site data where a complete year of both clearness index and horizontal diffuse could be obtained. Coefficients a and b were estimated by linear regression of 12 months of data. It is recognized that a and b values are approximate because of questions about the accuracy of diffuse measurements noted above. **Diffuse, DNR, and tilted surface results are not calculated using the Page method if latitudes are greater than 67^o North or South.** Low-light winter conditions cause large uncertainties in both insolation and diffuse data in late fall, winter, and early spring above those latitudes.

The technique employs an analysis of clearness index variance based on 12-month comparisons with all reference sites around the globe. The analysis is seasonally consistent in that winter months in a cell are compared with winter months in both hemispheres, etc. Values for coefficients a and b are taken from the closest-fitting (minimum 12-month variance) site. The analysis of variance process is repeated every 12 months over the 10-year period to allow a cell to select an alternative reference site if it is experiencing an abnormal year. The yearly a and b values were averaged and used to estimate Page-method diffuse fraction for the 1983-1993 10-year period. Additional information on application, results, and estimated uncertainty from the extended Page method can be found in Ref. [18]. The extended Page method inherently considers most climate regions over the globe for its results.

It should be noted that the seasonal variation correction suggested by Vignola and McDaniels (Ref. [19]) has not yet been attempted with the extended Page method. That procedure adds a third sine term to the above equation in the form of:

$$H_d/H = [a + (b*k) + (c*\sin(2\pi(n-40)/365))] \quad (6)$$

The period is a function of the day number of the year, n, and c is the maximum amplitude of the monthly residual during the 12-month period of the above analysis of variance procedure. Monthly residuals as well as a and b would have to be saved for the closest fitting reference site. They would be fitted to the above equation to estimate c and n. Vignola and McDaniels (Ref. [19]) demonstrated that the process reduced RMS uncertainty by about 25% when applied to six data sites in the Pacific Northwest Region of the United States. However, they recommend caution when using the above correction procedure outside the Pacific Northwest. They recommend testing the procedure at a large variety of locations with quality data in order to assess its general applicability. It is expected that additional site measurements may become available from the BSRN over the next few years for such a study.

5.2 Comparison of Diffuse Methods

It was decided that recent (1998-2000) research-grade, combined pyroheliometer/insolation site data would offer the best opportunity for accurate evaluation of Release 4 SSE diffuse and DNR results. Figure 10 shows locations of the sites for which NASA was able to obtain at least 12 consistent months of "good" data in time for validation of Release 4 products. Most data were received as monthly values. Only minute-scale or hourly were available for some sites, however. In these cases, results were accepted if (1) data were available for > 45 minutes of each hour, (2) > 8 hours of meaningful data existed each day, and (3) > 24 days of the month were available. Comparison with Fig. 1 indicates that desert/arid, steppe/semi-arid, temperate continental, subtropical land, tropical wetland, subtropical ocean, tropical ocean, as well as the convergence and stratus ocean regions are represented for latitudes between 43^o North and 15^o South. Missing were sites from tropical wet and dry land, boreal land, temperate ocean, and polar ocean. Data was obtained for polar land and coastal polar ocean/boreal land sites (the South Pole and Barrow, Alaska) that had a limited number of daylight months.

Satellite data are not yet available for the 1998-2000 period. The site-measured insolation was converted to monthly average values and input to SSE monthly average satellite methodologies for horizontal diffuse and DNR. These SSE-estimated values were then compared with site-measured values of horizontal diffuse and DNR. Uncertainty statistics for these two parameters

are optimistic because actual satellite-based values could not be used. Relative comparisons between Erbs et al. and Page/Staylor procedures are considered valid, however.

Figure 11 shows symbols and color codes that are used for each of the research-grade sites in Fig. 10. Figure 12 provides scatter charts and statistics that compare the Erbs et al. and extended Page methods. At first glance, both sets of results look comparable except that RETScreen has less scatter. Site-by-site analysis indicates that the Erbs et al. method provides a more accurate answer in those climate regions consistent with the four sites that ERBS et al. used for algorithm development (temperate continental, subtropical land, and steppe/semi-arid areas in Fig. 1).

Comparisons over all climate regions were performed using SSE satellite-based 10-year (July 1983 - June 1993) average horizontal insolation values as inputs. Figures 13 and 14 suggest that ERBS et al. results are smoother than the extended Page method over the globe. Figure 15 shows relative differences between the two methods as percent of horizontal diffuse fraction, (Page H_d - Erbs et al. H_d)/H. Both methods agree within about 15% for most of the globe where latitudes are less than approximately 55^o North or South and $0.3 \leq k \leq 0.8$.

A common issue between the two methods is that summer Sun elevation angles are low for latitudes greater than 55^o North or South, allowing for multi-direction, solar reflections from the bottoms of high clouds. This reflection adds to the diffuse radiation that is the result of light scattered through the clouds. The ERBS et al. method was developed in lower-latitude regions that may not experience cloud bottom reflection situations often. New research-grade pyroheliometer and horizontal insolation data from high-latitude regions are expected to be available from the BSRN in the future. It may be useful to verify or re-evaluate the Erbs et al. diffuse equations for these regions. It may be that coefficients of the cubic polynomial equations would be different in boreal and polar regions. A seasonal variation correction of the type suggested by Vignola and McDaniels (Ref. [19]) may be particularly important in high-latitude regions as well.

5.3 Monthly DNR Methods

5.3.1 RETScreen-type Method: This approach is a very slight variation of the RETScreen tilted surface radiation calculation and uses the "monthly average day" hourly calculation procedures employed by RETScreen (Ref. [15]) using Collares-Pereira and Rabl equations for insolation (Ref. [20]) and Liu and Jordan equations for diffuse radiation (Ref. [21]). [See equations (11) and (12) in Chapter 4 at RETScreen site <http//www.retscreen.net/ang/12.php>.] Specifically, the following equations were used to determine hourly horizontal surface insolation, $H_{h;}$ horizontal diffuse, H_{dh}; and horizontal beam, H_{bh}:

$$H_h = r_t H \quad (7)$$

$$H_{dh} = r_d H_d \quad (8)$$

$$H_{bh} = H_h - H_{dh} \quad (9)$$

$$DNR_h = H_{bh}/\cos\theta_{zh} \quad (10)$$

where:

H is from SSE.

H_d is from the Erbs et al. method.

$r_t = (\pi/24)*(A + B\cos\omega)*[(\cos\omega - \cos\omega_s)/(\sin\omega_s - \omega_s \cos\omega_s)]$ from Collares-Pereira and Rabl. (11)

$A = 0.409 + 0.5016 \sin[\omega_s - (\pi/3)]$ (12)

$B = 0.6609 + 0.4767 \sin[\omega_s - (\pi/3)]$ (13)

ω = solar hour angle for each daylight hour relative to solar noon between sunrise plus 30 minutes and sunset minus 30 minutes. The sun is displaced 15^o from the local meridian for each hour from local solar noon.

$r_d = (\pi/24)*[(\cos\omega - \cos\omega_s)/(\sin\omega_s - \omega_s \cos\omega_s)]$ from Liu and Jordan. (14)

$\cos\theta_{zh} = \cos(\text{latitude}) \cos(\text{solar declination}) \cos\omega + \sin(\text{latitude}) \sin(\text{solar declination})$ (15)

Hourly DNR values are summed to obtain DNR for the "monthly average day". It was recognized that such a procedure would be less accurate than using quality "day-by-day" site measurements, but RETScreen validation studies indicate that the "monthly average day" hourly calculation procedures give tilted surface results ranging within 3.9% to 8.9% of "day-by-day" hourly methods.

5.3.2 Extended Page/Empirical Staylor Hourly Method: This approach uses monthly horizontal insolation and diffuse radiation as follows:

$$H_b = H - H_d \quad (16)$$

$$DNR = H_b/\cos\theta_{zMT} \quad (17)$$

where:

H is from SSE.

H_d is from the extended Page method.

$$\cos\theta_{zMT} = f + g\,[(g - f)/ 2g]^{1/2} \quad (18)$$

= cosine of the solar zenith angle at the mid-time between sunrise and solar noon for the "monthly average day".

$$f = \sin(\text{latitude})\,\sin(\text{solar declination}) \quad (19)$$

$$g = \cos(\text{latitude})\,\cos(\text{solar declination}). \quad (20)$$

Beam radiation on a flat plate cannot be accurately related to direct normal values from sunrise to sunset by the average value of $\cos\theta_z$ over the daylight period (Vignola and McDaniels, Ref. [22]). The $\cos\theta_{zMT}$ equation was developed as an empirical approximation by Staylor as a part of his original method to compensate for that fact. $\text{Cos}\theta_{zMT}$ values can be quite different from average $\cos\theta_z$ (Gupta et al., Ref. [23]).

$$\text{average } \cos\theta_z = \{f \cos^{-1}(-f/g) + g[1 - (f/g)^2]^{1/2}\}/\cos^{-1}(-f/g) \quad (21)$$

5.4 Comparison of DNR Methods

Figure 16 provides scatter charts and statistics that compare the RETScreen and extended Page DNR methods for the sites between 43^o North and 15^o South. Again, results look comparable except that RETScreen has less scatter.

Comparisons over all climate regions were again performed using SSE satellite-based 10-year (July 1983 - June 1993) average horizontal insolation values as inputs. Figures 17 and 18 suggest that both methods are similar for much of the globe where latitudes are less than 50^o North. Figure 19 provides relative percent differences in DNR, (Page DNR-RETS DNR)/RETS DNR. Differences are less than 15% for most continental regions at latitudes less than 50^o in both hemispheres. Largest percent differences are in those regions with high solar zenith angles in the summer.

6. MONTHLY TILTED SURFACE RADIATION

6.1 Monthly Tilted Surface Methods

Tilted surface radiation is calculated with three monthly methods because no historical ground site data was available. The methods chosen may represent lower and upper bounds based on Duffie and Beckman, Ref. [14].

6.1.1 RETScreen Isotropic Diffuse Method: This isotropic diffuse method is used with 10-year average SSE insolation and RETScreen horizontal diffuse as inputs. Collares-Pereira and Rabl insolation eqn. (7) and Liu and Jordan diffuse eqn. (14) are again used to obtain hourly values for the "monthly average day". Hourly total radiation on a tilted surface, H_{th}, is estimated by the RETScreen tilt method from Ref. [15] on the "monthly average day" as:

H_{th} = solar beam component + sky diffuse component + surface/sky reflectance component

or

$$H_{th} = (H_h - H_{dh})R_{bh} + H_{dh}[(1+\cos\beta_h)/2] + H_h*\rho_s[(1-\cos\beta_h)/2] \quad (22)$$

where:

β_h = hourly slope of the PV array relative to a horizontal surface. β_h is constant for fixed panels or panels in a vertical- axis tracking system. $\beta_h = \theta_z$ for panels in a two-axis tracking system. Values for other types of tracking systems are given in Braun and Mitchell (ref. [24]).

ρ_s = surface reflectance or albedo is assumed to be 0.2 if temperature is above 0^oC or 0.7 if temperature is below -5^oC. Linear interpolation is used for temperatures between these values.

$$R_{bh} = \cos\theta_h/\cos\theta_{zh} \quad (23)$$

$\cos\theta_{zh}$ is from eqn. (15)

$$\cos\theta_h = \cos\theta_{zh}\cos\beta_h + (1 - \cos\theta_{zh})(1 - \cos\beta_h)(\cos(\gamma_{sh} - \gamma_h)) \quad (24)$$

where:

$\gamma_{sh} = \sin^{-1}[(\sin\omega\cos(\text{solar declination}))/\sin\theta_{zh}]$

= hourly solar azimuth; angle between the line of sight of the Sun into the horizontal surface and the local meridian. Azimuth is zero facing the equator, positive west, and negative east.

γ_h = hourly surface azimuth of the tilted surface; angle between the projection of the normal to the surface into the horizontal surface and the local meridian. Azimuth is zero facing the equator, positive west, and negative east. γ_h is constant for fixed surfaces. $\gamma_h = \gamma_{sh}$ for both vertical- and two-axis tracking systems. See Ref. [24] for other types of tracking systems.

Monthly average tilted surface radiation, H_t, is estimated by summing H_{th} over the "monthly average day".

6.1.2 Perez Non-Isotropic/Extended Page Horizontal Diffuse Method: The non-isotropic diffuse method of Perez et al. (Ref. [25]) is used with 10-year average SSE insolation and extended Page horizontal diffuse as inputs. Collares-Pereira and Rabl insolation eqn. (7) and Liu and Jordan diffuse eqn. (14) are again used to obtain hourly values for the "monthly average day". The Perez tilt equation, F factors, etc. are applied to "monthly average day" parameters in an hourly equation similar to eqn. (22). The solar beam and surface/sky reflectance components are identical, however, the sky diffuse component is based on the non-isotropic diffuse method of Perez et al. (Ref. [25]). The new hourly tilted surface equation is:

$$H_{th} = (H_h - H_{dh})R_{bh} + H_{dh}[((1-F_{1h})(1+\cos\beta_h)/2) + F_{1h}(a_h/b_h) + F_{2h}\sin\beta_h] + H_h*\rho_s[(1-\cos\beta_h)/2] \quad (25)$$

where:

ρ_s is taken from global monthly average, satellite-based SSE albedo for preliminary estimates. The examples in Fig. 2 of Ineichen, et al. (Ref. [26]) suggest that local values of albedo can be important for tilted surface radiation. Final-design tilt estimates should be based on the albedo of the local area.

$a_h = \cos\theta_h$ or zero, whichever is maximum. (26)

$b_h = \cos\theta_{zh}$ or 0.087, whichever is maximum. (27)

Coefficients which lead to the F_{1h} and F_{2h} (circumsolar and horizon brightening coefficients, respectively) are based on experimental measurements from 10 U.S. and 3 European sites from 30^o to 50^o North latitudes. Climate regions included

steppe/semi-arid, desert/arid, temperate continental, subtropical land, temperate ocean, and highly polluted environments (Fig. 1 and Ref. [25]). The experimental data consisted of simultaneous measurements of global, vertical surface, tilted surface (various azimuths), and direct-normal values for both solar radiation and illuminance. The solar radiation measurements were synthesized with hourly parameters Ep_h, Del_h, and θ_{zh} where:

$$Ep_h = (((H_{dh} + H)/H_{dh})+(1.041\theta_{zh}^3))/(1+(1.041\theta_{zh}^3)) \quad (28)$$

= sky clearness, range = 1.0 (overcast) to 6.2 (clear sky)

$$Del_h = H_{dh}/(\cos\theta_{zh}) \quad (29)$$

= sky brightness

$$\theta_{zh} = \text{solar zenith angle (radians)} \quad (30)$$

Given hourly values of Ep_h, Del_h, and θ_{zh}, values for coefficients F11 through F12 are determined from Table 2. Hourly values for F1h and F2h are determined from:

$$F1h = F11 + (F12*Del_h) + (F13*\theta_{zh}) \quad (31)$$

$$F2h = F21 + (F22*Del_h) + (F23*\theta_{zh}) \quad (32)$$

Monthly average tilted surface radiation, H_t, is estimated by summing H_{th} over the "monthly average day".

6.1.3 Perez Non-Isotropic/Erbs et al. Horizontal Diffuse Method: This approach uses the Erbs et al. method [equations (1) through (4)] to estimate monthly H_d. That H_d is converted to "monthly average day" hourly values, H_{dh}, using the Liu and Jordan diffuse method in equations (8) and (14). Again, SSE monthly H is converted into "monthly average day" hourly values, H_h, using the Collares-Pereira and Rabl equations (7), (11), (12), and (13).

The SSE/RETScreen-based hourly values of H_h and H_{dh} are then applied to Perez et al. equations (25) through (32) to obtain non-isotropic tilted surface radiation estimates.

6.2 Comparison of Tilted Surface Radiation Methods

Tables 3 through 5 show the results of tilted surface calculations for the region near Sacramento, California calculated by the three methods. Row 4 (Tilt 0) is the result for a horizontal surface after processing of the equations and integrating over the "monthly average day". Results are close, but do not agree with input values from row 1 (SSE horizontal insolation) because of approximations in the other inputs and time integration inaccuracies. Tables 6 through 11 provide Equivalent Sun Hours and Peak Sun Hours using minimum and maximum SSE horizontal insolation values as input.

Optimum tilt angles are different between the three methods as expected from the discussion in Duffie and Beckman (Ref. [14]). Tilt method differences are caused by differences between the diffuse and DNR inputs as well as the effect of isotropic versus non-isotropic diffuse skylight assumptions. It should be noted that tilted surface radiation tables provided in the SSE web site have an additional two rows giving optimum angle and solar radiation for each month. Radiance values are summed to provide an estimate of yearly improvement if tilt angles are adjusted to optimum values each month.

SSE has not been able to obtain a variety of tilted surface measurements to test computed values. SSE RETScreen-type tilt estimates have been tested against computations using the actual RETScreen software from the RETScreen CD-ROM. SSE Perez-based tilt estimates were tested against NREL Solar Radiation Data Base (SRDB) results (Refs. [27, 28]) for Sacramento, CA as shown in Fig. 20. NREL monthly horizontal global and diffuse values were input to the SSE Perez Non-Isotropic/Extended Page Horizontal Diffuse Method. Results suggest that the SSE application of Perez et al. equations on "monthly average day" basis produces similar results to those obtained by NREL using the more accurate day-by-day application of the method.

In general, SSE will not estimate the same horizontal insolation and diffuse values as given in SRDB. SSE horizontal insolation is a 10-year average value, and SSE horizontal diffuse is estimated by two methods, Erbs et al. and extended Page. The top chart in Fig. 21 shows insolation and diffuse differences between SSE and SRDB at Sacramento, CA. The middle and

lower charts show tilted surface differences between SRDB and the three SSE tilted surface methods. Tilt-value differences appear most significant in winter for the Sacramento location.

Figures 22 through 24 provide total solar radiation values for stationary surfaces tilted toward the equator at the latitude angle for each of the three SSE methods. **Tilted surface radiation calculations are not performed in winter conditions if there are less than 4 hours of daylight**. Comparison of tilt values with horizontal surface values in Fig. 5 demonstrates significant changes that usually occur at locations far north or south of the equator if tilted solar panel surfaces are used. Large shifts in summer to winter cloud cover may modify these effects in some locations, however.

Individual comparisons of Figs. 22, 23, and 24 show differences between the methods depending on location. Figures 25 and 26 compare results between three SSE methods as a percent of RETScreen tilt values. Tilt values for the methods appear to agree within 15 percent for mid-summer latitude angles as high as 75 degrees. Differences begin to exceed 15 percent in mid-winter when latitudes approach 40^{o} to 55^{o}, depending on method.

7. WIND SPEED PARAMETERS

Release 4 SSE winds are based on the Version 1 GEOS (GEOS-1) reanalysis data set described in Takacs, Molod, and Wang (Ref. [29]). Fifty-meter velocities were derived from layer 1 values using equations provided to SSE by GEOS-1 project personnel.

Adjustments were made in a few regions based on science information from Dorman and Sellers (Ref. [30]) and recent vegetation maps developed by the International Geosphere and Biosphere Project (IGBP) (Fig. 27). GEOS-1 vegetation maps were compared with IGBP vegetation maps. Significant differences in the geographic distribution of crops, grasslands, and savannas were found in a few regions. In those regions, airport data were converted to new 50-m height velocities based on procedures in Gipe (Ref. [31]). GEOS-1 50-m values were replaced with the new Gipe-derived estimates in those regions. Ten-year annual average maps of 50-m and 10-m "airport" wind speeds are shown in Fig. 28. Velocity magnitude changes are now consistent with general vegetation heights that might be expected from the scene types in Fig. 27. Note that SSE heights are above the soil, water, or ice surface and not above the "effective" surface in the upper portion of vegetation canopies.

Ten-year average SSE "airport" estimates were compared with 30-year average airport data sets over the globe furnished by the RETScreen project. In general, monthly bias values varied between $\pm$0.2 m/s and RMS (including bias) values range around 1.3 m/s (Fig. 29). This represents a 20 to 25 percent level of uncertainty relative to mean monthly values. That is about the same level of uncertainty quoted by Schwartz (Ref. [32]). Gipe (Ref. [31]) notes that operational wind measurements are sometimes inaccurate for a variety of reasons. Site-by-site comparisons at nearly 790 locations indicate SSE 10-m "airport" winds tend to be higher than airport measurements in remote desert regions in some foreign countries. SSE values are usually lower than measurements in mountain regions where localized accelerated flow may occur at passes, ridgelines or mountain peaks. One-degree resolution wind data is not an accurate predictor of local conditions in regions with significant topography variation or complex water/land boundaries.

Designers of "small-wind" power sites need to consider the effects of vegetation canopies effecting wind from either some or all directions. Trees and shrub-type vegetation with various heights and canopy-area ratios reduce near-surface velocities by different amounts. GEOS-1 calculates 10-m velocities for a number of different vegetation types. Values are calculated by parameterizations developed from a number of "within-vegetation" experiments in Canada, Scandinavia, Africa, and South America. The ratio of 10-m to 50-m velocities (V10/V50) for 17 vegetation types is provided in table 12. All values were taken from GEOS-1 calculations except for the "airport" flat rough grass category that was taken from Gipe.

8. TEMPERATURE, PRESSURE, AND HUMIDITY PARAMETERS

8.1 Near-surface Air Temperature

Year 1986 is considered to have had near-average weather. SSE 10-meter air temperatures for 1986 were compared to 30-year monthly average RETScreen weather data from 1000+ ground sites over the globe. Original GEOS-1 temperatures are known to be less accurate in cold climates. SSE performed an approximate linear correction in the range 223 K to 273 K to bring values over the globe in line with 30-year RETScreen values. Ten-year average SSE values of these parameters have been compared with 30-year RETScreen values in the upper chart of Fig. 30. Unfortunately, uncertainty on a global scale is still larger for cold temperatures. Generally, RETScreen temperatures are warmer than SSE temperatures.

Near-surface air temperature is a property that is converted into a number of design parameters in the renewable energy industry. An analysis of the effects of the above near-surface air temperature uncertainty on temperature-related hardware design parameters has been performed by RETScreen personnel. A sample of approximately 200 potential renewable energy sites in 7 continental regions has been selected for most parameters. The Heating degree-days parameter was calculated at 100 potential cold-weather sites. Ten-year average SSE values of these parameters have been compared with 30-year RETScreen values. Results provided by RETScreen are as follows:

Parameter	Estimated Uncertainty (Includes Bias)
10-m Air Temperature, K	1.2%
Heating Design Temperature, K	1.3%
Cooling Design Temperature, K	1.4%
Summer Mean Daily Temperature Range, K	0.9%
Heating Degree-Days Below 18-deg C, deg-days	15.0%

8.2 Surface Air Pressure

SSE surface air pressure and RETScreen values were correlated over the globe with an estimated uncertainty of 3.8% as shown in Fig. 30, bottom chart. Bias differences average -1.5% with RETScreen values higher than SSE values. Surface air pressure was also tested using the 200 potential renewable sites in 7 continental regions. Estimated uncertainty is 2.4%. Most regions have similar values except the Southwest Pacific and South America experience 1.2% and 5.4% uncertainty, respectively.

8.3 Relative Humidity

Relative humidity is not available from NASA GEOS-1 data. An approximation technique to estimate values was developed for use in Release 3 SSE. The procedure uses surface pressure, 10-meter temperature, and 10-meter specific humidity. Ten-year SSE results were correlated with approximately 820 RETScreen 30-year values over the globe. Estimated global uncertainty is 18.5% of the mean value of the 820 sites as shown in Fig. 31. SSE uncertainties are higher than RETScreen. Relative humidity was also tested using the 200 potential renewable energy sites in 7 continental regions. Average estimated uncertainty is approximately 10% of the mean value of those 200 sites.

8.4 Precipitation

Ten-year monthly average 1^o x 1^o global precipitation data was derived from the Global Precipitation Climatology Project (GPCP) Version 2 Combined Precipitation Data Set (Ref. [33]). The GPCP combined precipitation data were provided by the NASA/Goddard Space Flight Center's Laboratory for Atmospheres, which develops and computes the data. Monthly averaged GPCP data for each year were averaged for the 10-year period from July 1983 through June 1993. The 2.5^o x 2.5^o GPCP data were interpolated to 1^o x 1^o using a bilinear algorithm. Units are in millimeters/day.

9. REFERENCES

[1] Whitlock, C. H., D. R. Cahoon, and T. Konzelmann, 1996: Biomass Burning Effects on Shortwave Radiation in Africa. Biomass Burning and Global Change. J. S. Levine, Ed., MIT Press, Cambridge, pp. 485-491.

[2] Smith, G. L., A. C. Wilber, S. K. Gupta, and P. W. Stackhouse, Jr., 2002: Surface Radiation Budget and Climate Classification, Applied Optics, Vol. 15, pp. 1175-1188.

[3] Pinker, R. T. and I. Laszlo, 1992: Modeling Surface Solar Irradiance for Satellite Application on a Global Scale. Journal of Applied Meteorology, Vol. 31, pp. 194-211.

[4] ISCCP information can be obtained from <http://isccp.giss.nasa.gov/>.

[5] Data Assimilation Office information can be obtained from <http://gmao.gsfc.nasa.gov/>.

[6] Whitlock, Charles H., Donald E. Brown, William S. Chandler, Roberta C. DiPasquale, Shashi K. Gupta, Anne C. Wilber, Nancy A. Ritchey, David P. Kratz, and Paul W. Stackhouse, 2001: Global Solar Energy Anomalies Including El Nino and La Nina Years. ASME Journal of Solar Energy Engineering, Vol. 23, No. 3, pp. 211-215.

[7] Vignola, F. and D. K. McDaniels, 1984: Correlations Between Diffuse and Global Insolation for the Pacific Northwest. Solar Energy, Vol. 32, No. 2, pp. 161-168.

[8] LeBaron, B. A., J. J. Michalsky, and R. Perez, 1990: A Simple Procedure for Correcting Shadowband Data for All Sky Conditions. Solar Energy, Vol. 44, No. 5, pp. 249-256.

[9] Haeffelin, M, S. Kato, A.M. Smith, C. K. Rutledge, T. P. Charlock, and J. R. Mahan, 2001: Determination of the Thermal Offset of the Eppley Precision Spectral Pyranometer, Applied Optics, Vol. 40, pp. 472-484.

[10] Michalsky, Joseph J., 2002: Comparison of Diffuse Shortwave Irradiance Measurements. Paper 7.1, 11th Conference on Atmospheric Radiation, American Meteorological Society, Ogden, Utah, June 3-7.

[11] Philipona, Rolf, 2002: Substantial Underestimation of Solar Global and Diffuse Radiation Caused by Pyranometer Thermal Offsets. Paper 7.3, 11th Conference on Atmospheric Radiation, American Meteorological Society, Ogden, Utah, June 3-7.

[12] Dutton, E. G., J. J. Michalsky, T. Stoffel, B. W. Forgan, J. Hickey, D. W. Nelson, T. L. Alberta, and I. Reda, 2001: Measurement of Broadband Diffuse Irradiance Using Current Commercial Instrumentation with a Correction for Thermal Offset Errors. Journal of Atmospheric and Oceanic Technology, Vol. 18, pp. 297-314.

[13] Erbs, D. G., S. A. Klein, and J. A. Duffie, 1982: Estimation of the Diffuse Radiation Fraction for Hourly, Daily and Monthly average Global Radiation. Solar Energy, Vol. 28, No. 4, pp. 293-302.

[14] Duffie, J. A. and W. A. Beckman, 1991: Solar Engineering of Thermal Processes, Second Edition, John Wiley & Sons, Inc., New York.

[15] Leng, G., N. Meloche, A. Monarque, G. Painchaud, D. Thevenard, M. Ross, and P. Hosette, 2002: Chapter 4, Photovoltaic Project Analysis, Renewable Energy Project Analysis: RETScreen Engineering & Cases, CANMET Energy Technology Centre - Varennes, Canada. (Forthcoming university textbook, see preliminary electronic version at <http://www.retscreen.net/ang/12.php>).

[16] Page, J. K., 1964: The Estimation of Monthly Mean Values of Daily Total Shortwave Radiation on Vertical and Inclined Surfaces From Sunshine Records for Latitudes 40^{o}N - 40^{o}S, Proceedings of the United Nations Conference On New Sources of Energy; Solar Energy, Wind Power and Geothermal Energy.

[17] Brunger, A. and D. Thevenard, 1999: Evaluation of Models for Natural Illumination on Horizontal Surfaces, Proceedings of the North Sun 1999 Conference, Solar Energy Society of Canada, Inc.

[18] Whitlock, C.H., D. E. Brown, R.C. DiPasquale, W. S. Chandler, and P. W. Stackhouse, 2002: Variability of Diffuse Solar Surface Radiation over the Globe. SOLAR | 2002, Paper 189A, Proceedings of Sunrise on the Reliable Energy Economy, June 15-19, Reno, NV. Sponsored by ASES and 12 other industry societies.

[19] Vignola, F. and D. K. McDaniels, 1984: Diffuse-Global Correlations: Seasonal Variations. Solar Energy, Vol. 33, No. 5, pp. 397-402.

[20] Collares-Pereira, M. and A. Rabl, 1979: The Average Distribution of Solar Radiation- Correlations Between Diffuse and Hemispherical and Between Daily and Hourly Insolation Values. Solar Energy, Vol. 22, No. 1, pp. 155-164.

[21] Liu, B. Y. H. and R. C. Jordan, 1960: The Interrelationship and Characteristic Distribution of Direct, Diffuse, and Total Solar Radiation. Solar Energy, Vol. 4, No. 3, pp. 1-19.

[22] Vignola, F. and D. K. McDaniels, 1984: Transformation of Direct Solar Radiation to Tilted Surfaces. Proceedings of the 1984 Annual Meeting of the American Solar Energy Society, Inc. Anaheim, CA, pp. 651-655.

[23] Gupta, S. K., D. P. Kratz, P. W. Stackhouse, Jr., and A. C. Wilber, 2001: The Langley Parameterized Shortwave Algorithm (LPSA) for Surface Radiation Budget Studies. National Aeronautics and Space Administration TP-2001-211272, 31 p. Available NASA CASI, telephone (301) 621-0390.

[24] Braun, J. E. and J. C. Mitchell, 1983: Solar Geometry for Fixed and Tracking Surfaces. Solar Energy, Vol. 31, No. 5, pp. 439-444.

[25] Perez, Richard, Pierre Ineichen, Robert Seals, Joseph Michalsky, and Robert Stewart, 1990: Modeling Daylight Availability and Irradiance Components from Direct and Global Irradiance. Solar Energy, Vol. 44, No. 5, pp. 271-289.

[26] Ineichen, Pierre, Richard Perez, and Robert Seals, 1987: The Importance of Correct Albedo Determination for Adequately Modeling Energy Received by Tilted Surfaces. Solar Energy, Vol. 39, No. 4, pp. 301-305.

[27] Marion, William and Stephen Wilcox, 1994: Solar Radiation Data Manual: Solar Radiation Data Manual for Flat-Plate and Concentrating Collectors, NREL/TP-463-5607, DE93018229.

[28] Marion, William and Stephen Wilcox, 1995: Solar Radiation Data Manual: Solar Radiation Data Manual for Flat-Plate and Concentrating Collectors, NREL/TP-463-7904, DE95009254.

[29] Takacs, L. L., A. Molod, and T. Wang, 1994: Volume 1: Documentation of the Goddard Earth Observing System (GEOS) general circulation model - version 1, NASA Technical Memorandum 104606, Vol. 1, 100 pp.

[30] Dorman, J. L. and P. J. Sellers, 1989: A Global Climatology of Albedo, Roughness Length and Stomatal Resistance for Atmospheric General Circulation Models as Represented by the Simple Biosphere Model (SiB). Journal of Atmospheric Science, Vol. 28, pp. 833-855.

[31] Gipe, Paul, 1999: Wind Energy Basics, Chelsea Green Publishing, 122pp.

[32] Schwartz, Marc, 1999: Wind Energy Resource Estimation and Mapping at the National Renewable Energy Laboratory. NREL Conf. Pub. NREL/CP-500-26245.

[33] Huffman, George J., R. F. Adler, P. Arkin, A. Chang, R. Ferraro, A. Gruber, J. Janowiak, A. McNab, B. Rudolf, U. Schneider, 1997: The Global Precipitation Climatology Project (GPCP) Combined Precipitation Dataset. Bulletin of the American Meteorological Society: Vol. 78, No. 1, pp. 5-20.

Table 1. Reference-site clearness index table used to extend the Page method.

SITE	LAT	LON	Coef A	Coef B	JAN	FEB	MAR	APR	MAY	JUN	JUL	AUG	SEP	OCT	NOV	DEC
Albuquerque, NM	35.08	-106.65	0.92	-0.96	0.57	0.62	0.59	0.63	0.60	0.60	0.59	0.56	0.64	0.60	0.59	0.54
Anchorage, AK	61.22	-149.90	1.28	-1.51	0.27	0.34	0.35	0.40	0.38	0.40	0.39	0.37	0.35	0.33	0.33	0.26
Boulder, CO	40.00	-105.27	1.01	-1.18	0.51	0.53	0.52	0.55	0.54	0.57	0.56	0.56	0.64	0.61	0.51	0.50
Chicago, IL	41.85	-87.85	1.15	-1.34	0.37	0.44	0.42	0.47	0.51	0.52	0.50	0.52	0.55	0.50	0.38	0.35
Columbia, SC	34.00	-81.03	1.03	-1.16	0.45	0.50	0.49	0.52	0.55	0.53	0.53	0.52	0.53	0.54	0.52	0.49
Columbus, OH	39.95	-82.98	1.26	-1.56	0.36	0.42	0.41	0.45	0.47	0.50	0.48	0.50	0.53	0.47	0.39	0.36
Davos, CH	46.81	9.82	1.00	-1.01	0.35	0.37	0.39	0.37	0.43	0.43	0.50	0.50	0.48	0.41	0.36	0.34
Geneve, CH	46.21	6.14	0.90	-0.90	0.32	0.35	0.37	0.37	0.40	0.40	0.46	0.46	0.44	0.36	0.33	0.31
Locarno, CH	46.18	8.90	0.76	-0.64	0.34	0.37	0.39	0.38	0.43	0.43	0.50	0.50	0.48	0.41	0.35	0.33
Los Angeles, CA	34.05	-118.23	0.98	-1.04	0.57	0.62	0.59	0.63	0.62	0.61	0.62	0.62	0.64	0.59	0.61	0.56
San Francisco, CA	37.77	-122.42	0.96	-1.08	0.53	0.56	0.56	0.61	0.61	0.60	0.61	0.56	0.61	0.56	0.55	0.52
San Juan, PR	18.47	-66.10	1.22	-1.44	0.63	0.64	0.65	0.64	0.59	0.56	0.56	0.57	0.56	0.56	0.57	0.61
Zurich, CH	47.38	8.54	1.07	-1.18	0.34	0.38	0.39	0.40	0.44	0.42	0.49	0.49	0.46	0.40	0.33	0.32
ARM Ctr. Fac. (OK)	36.60	-97.48	0.61	-0.45	0.39	0.59	0.48	0.54	0.58	0.49	0.66	0.63	0.56	0.59	0.63	0.53
Manus	-2.06	147.43	0.44	0.01	0.54	0.52	0.52	0.54	0.52	0.51	0.52	0.52	0.56	0.58	0.52	0.42
Florianapolis, Brazil	-27.53	-48.52	0.97	-0.89	0.42	0.40	0.47	0.49	0.51	0.55	0.42	0.39	0.33	0.39	0.49	0.55
Tateno, Japan	36.05	140.13	0.29	0.38	0.50	0.48	0.51	0.35	0.41	0.28	0.34	0.27	0.22	0.38	0.51	0.49
Chesapeake Light	36.90	-75.71	-0.02	0.75	0.46	0.37	0.55	0.41	0.54	0.55	0.37	0.53	0.51	0.62	0.48	0.50
Saudi Solar Village	24.91	46.41	0.34	-0.04	0.59	0.54	0.66	0.67	0.68	0.71	0.71	0.69	0.69	0.69	0.67	0.63
Bondville, IL	40.06	-88.37	0.83	-0.77	0.42	0.40	0.55	0.40	0.53	0.52	0.63	0.58	0.62	0.54	0.55	0.46
Desert Rock, NV	36.63	-116.02	0.83	-0.88	0.62	0.63	0.70	0.62	0.72	0.75	0.69	0.71	0.71	0.74	0.66	0.66
Fort Peck, MT	48.31	-105.10	0.88	-0.86	0.52	0.56	0.56	0.52	0.51	0.58	0.62	0.60	0.51	0.50	0.54	0.53
Goodwin Creek, MS	34.25	-89.87	0.57	-0.39	0.37	0.48	0.48	0.52	0.58	0.51	0.59	0.64	0.58	0.60	0.62	0.48
Penn State College,	40.72	-77.93	0.50	-0.10	0.36	0.41	0.52	0.48	0.54	0.51	0.55	0.50	0.50	0.50	0.44	0.35
Table Mountain, CO	40.13	-105.24	0.56	-0.37	0.53	0.66	0.66	0.51	0.59	0.57	0.57	0.54	0.57	0.60	0.63	0.59
Barrow, AK	71.32	-156.95	-0.06	2.34	0.30	0.33	0.51	0.56	0.53	0.50	0.40	0.30	0.29	0.24	0.91	n/a
Bermuda	32.30	-64.33	0.91	-1.00	0.41	0.38	0.38	0.48	0.54	0.58	0.53	0.54	0.52	0.46	0.46	0.34
Kwajalein	8.72	-167.73	0.62	-0.45	0.50	0.52	0.52	0.54	0.57	0.45	0.44	0.50	0.47	0.43	0.41	0.51
SouthPole	-90.00	0.00	0.16	0.70	0.79	0.72	0.52	n/a	n/a	n/a	n/a	n/a	0.58	0.59	0.76	0.82
Samoa	-14.23	-170.56	0.41	-0.17	0.37	0.37	0.44	0.47	0.35	0.43	0.46	0.53	0.47	0.44	0.47	0.50
WRDC Ref Site 1	-12.90	40.50	1.03	-1.13	0.52	0.53	0.48	0.64	0.68	0.60	0.60	0.66	0.64	0.64	0.67	0.63
WRDC Ref Site 2	-19.80	34.90	0.79	-0.91	0.59	0.56	0.61	0.64	0.69	0.62	0.59	0.62	0.63	0.64	0.52	0.62
WRDC Ref Site 3	-20.80	55.51	0.65	-0.57	0.57	0.56	0.58	0.61	0.59	0.63	0.62	0.56	0.58	0.60	0.56	0.50
WRDC Ref Site 4	-22.20	114.00	0.74	-0.77	0.72	0.69	0.73	0.70	0.67	0.56	0.64	0.74	0.75	0.77	0.74	0.75
WRDC Ref Site 5	-24.80	113.60	0.66	-0.65	0.72	0.67	0.71	0.61	0.63	0.57	0.60	0.70	0.70	0.73	0.71	0.75
WRDC Ref Site 6	-26.60	118.50	0.71	-0.73	0.68	0.67	0.71	0.61	0.63	0.57	0.66	0.74	0.74	0.78	0.70	0.74
WRDC Ref Site 7	-27.40	153.00	0.74	-0.76	0.54	0.54	0.50	0.43	0.56	0.61	0.59	0.59	0.59	0.63	0.61	0.51
WRDC Ref Site 8	-33.80	121.80	0.72	-0.58	0.65	0.52	0.47	0.47	0.48	0.43	0.48	0.45	0.44	0.55	0.52	0.60
WRDC Ref Site 9	-33.90	151.10	0.46	-0.21	0.47	0.44	0.48	0.41	0.47	0.54	0.52	0.54	0.55	0.56	0.65	0.61
WRDC Ref Site 10	-34.90	138.50	0.85	-0.85	0.67	0.71	0.54	0.57	0.52	0.43	0.48	0.55	0.61	0.57	0.58	0.65
WRDC Ref Site 11	-42.80	147.50	0.46	-0.10	0.52	0.59	0.51	0.50	0.54	0.43	0.48	0.48	0.50	0.58	0.52	0.47
WRDC Ref Site 12	1.37	103.90	0.55	-0.04	0.49	0.52	0.42	0.44	0.42	0.46	0.48	0.45	0.47	0.44	0.44	0.45
WRDC Ref Site 13	19.33	-99.10	0.92	-1.10	0.59	0.58	0.57	0.53	0.55	0.51	0.45	0.49	0.46	0.47	0.60	0.60
WRDC Ref Site 14	23.13	113.30	0.61	-0.08	0.44	0.20	0.12	0.20	0.27	0.30	0.41	0.42	0.41	0.51	0.43	0.38
WRDC Ref Site 15	25.01	102.60	0.71	-0.42	0.56	0.52	0.45	0.48	0.35	0.29	0.30	0.54	0.39	0.31	0.53	0.55
WRDC Ref Site 16	30.61	114.10	0.71	-0.18	0.39	0.40	0.23	0.39	0.42	0.35	0.52	0.51	0.34	0.44	0.46	0.34
WRDC Ref Site 17	31.16	121.40	0.48	0.05	0.32	0.23	0.40	0.39	0.38	0.45	0.52	0.43	0.36	0.40	0.40	0.40
WRDC Ref Site 18	38.00	-1.16	0.95	-0.95	0.50	0.61	0.64	0.55	0.60	0.55	0.67	0.64	0.65	0.58	0.49	0.59
WRDC Ref Site 19	39.46	-6.33	0.65	-0.51	0.56	0.55	0.59	0.52	0.59	0.66	0.67	0.62	0.58	0.54	0.37	0.31
WRDC Ref Site 20	4.83	-52.30	0.98	-1.02	0.34	0.37	0.40	0.44	0.36	0.41	0.55	0.60	0.61	0.55	0.48	0.45
WRDC Ref Site 21	4.93	114.90	0.34	0.13	0.42	0.49	0.42	0.44	0.38	0.38	0.39	0.36	0.39	0.43	0.41	0.48
WRDC Ref Site 22	41.26	69.26	1.08	-1.02	0.45	0.47	0.47	0.60	0.59	0.64	0.71	0.73	0.66	0.67	0.45	0.33
WRDC Ref Site 23	42.46	-2.38	0.66	-0.39	0.40	0.48	0.52	0.44	0.52	0.59	0.60	0.59	0.55	0.53	0.35	0.33
WRDC Ref Site 24	43.35	-5.86	0.52	-0.13	0.43	0.45	0.41	0.43	0.47	0.35	0.40	0.40	0.39	0.30	0.41	0.30
WRDC Ref Site 25	43.78	87.61	0.68	-0.59	0.34	0.46	0.37	0.51	0.53	0.57	0.53	0.55	0.60	0.49	0.39	0.33
WRDC Ref Site 26	46.76	-56.10	0.93	-0.99	0.32	0.34	0.42	0.37	0.49	0.40	0.34	0.44	0.50	0.40	0.29	0.38
WRDC Ref Site 27	48.76	2.02	0.60	-0.16	0.28	0.35	0.29	0.47	0.37	0.44	0.45	0.50	0.35	0.37	0.39	0.18
WRDC Ref Site 28	52.01	113.30	0.80	-0.63	0.53	0.56	0.65	0.55	0.57	0.62	0.50	0.48	0.47	0.60	0.52	0.48
WRDC Ref Site 29	52.28	20.96	0.66	-0.13	0.23	0.32	0.39	0.54	0.54	0.45	0.54	0.47	0.36	0.48	0.32	0.21
WRDC Ref Site 30	52.96	158.70	0.50	0.10	0.39	0.39	0.56	0.53	0.50	0.33	0.43	0.47	0.51	0.46	0.45	0.45
WRDC Ref Site 31	53.63	10.00	0.67	-0.29	0.19	0.33	0.34	0.45	0.51	0.32	0.41	0.45	0.31	0.37	0.19	0.22
WRDC Ref Site 32	54.93	73.40	1.22	-1.20	0.39	0.47	0.59	0.57	0.67	0.59	0.56	0.44	0.47	0.50	0.43	0.47
WRDC Ref Site 33	57.20	-3.83	1.21	-1.46	0.27	0.37	0.36	0.48	0.44	0.32	0.45	0.38	0.38	0.31	0.28	0.25
WRDC Ref Site 34	59.36	13.46	0.86	-0.71	0.24	0.25	0.45	0.47	0.57	0.49	0.47	0.47	0.37	0.35	0.36	0.28
WRDC Ref Site 35	64.58	40.50	0.65	0.22	0.40	0.34	0.53	0.40	0.36	0.42	0.48	0.52	0.32	0.27	0.21	0.44
WRDC Ref Site 36	65.78	87.9	1.38	-1.30	0.35	0.40	0.57	0.47	0.47	0.42	0.51	0.40	0.38	0.30	0.27	0.44
WRDC Ref Site 37	67.55	133.30	0.54	0.35	0.33	0.45	0.63	0.63	0.55	0.43	0.61	0.43	0.43	0.43	0.44	0.00
WRDC Ref Site 38	68.50	112.40	1.24	-0.58	0.50	0.44	0.62	0.56	0.62	0.45	0.54	0.34	0.50	0.49	0.58	0.58
WRDC Ref Site 39	69.75	27.03	0.34	1.13	0.40	0.38	0.51	0.52	0.42	0.32	0.42	0.36	0.40	0.37	0.26	0.26
Leopoldville, Zaire	-4.18	15.18	1.03	-1.21	0.43	0.47	0.49	0.49	0.51	0.53	0.52	0.50	0.48	0.44	0.42	0.42
Capetown, S. Africa	-33.48	18.28	1.02	-1.26	0.66	0.63	0.61	0.59	0.57	0.57	0.56	0.58	0.57	0.61	0.63	0.64
Darban, S. Africa	-29.48	31.00	1.10	-1.43	0.52	0.51	0.53	0.60	0.62	0.62	0.62	0.59	0.53	0.49	0.48	0.50
Windhoek, Namibia	-22.05	17.10	0.88	-0.95	0.58	0.57	0.60	0.64	0.68	0.71	0.71	0.72	0.70	0.70	0.62	0.62
Pretoria, S. Africa	-25.43	28.16	0.98	-1.16	0.56	0.53	0.55	0.63	0.67	0.67	0.68	0.66	0.62	0.58	0.55	0.53

Table 2. F11 through F23 irradiance coefficients from Perez et al. (ref. [25]).

Ep Range	F11	F12	F13	F21	F22	F23
1.000 - 1.065	-0.008	0.588	-0.062	-0.060	0.072	-0.022
1.065 - 1.230	0.130	0.683	-0.151	-0.019	0.066	-0.029
1.230 - 1.500	0.330	0.487	-0.221	0.055	-0.064	-0.026
1.500 - 1.950	0.568	0.187	-0.295	0.109	-0.152	-0.014
1.950 - 2.800	0.873	-0.392	-0.362	0.226	-0.462	0.001
2.800 - 4.500	1.132	-1.237	-0.412	0.288	-0.823	0.056
4.500 - 6.200	1.060	-1.600	-0.359	0.264	-1.127	0.131
6.200 →	0.678	-0.327	-0.250	0.156	-1.377	0.251

Table 3. Average Tilted Surface Radiation using RETScreen Isotropic Diffuse Method (kWhr/m^2/day).
Sacramento, CA, Latitude 38.5^o N, Longitude 121.5^o W, Tilt toward South.

Month	**1**	**2**	**3**	**4**	**5**	**6**	**7**	**8**	**9**	**10**	**11**	**12**	**Avg**
SSE HRZ	2.11	3.26	4.48	6.13	7.27	7.83	7.45	6.61	5.32	3.88	2.58	1.91	4.90
ERBS DIF	0.88	1.11	1.63	1.90	2.06	2.10	2.11	1.95	1.70	1.36	0.93	0.80	1.54
RET DNR	3.17	4.31	5.03	6.87	7.65	8.11	7.68	7.23	5.92	5.22	3.97	3.10	5.69
Tilt 0	2.09	3.17	4.44	6.10	7.23	7.77	7.40	6.59	5.24	3.85	2.55	1.90	4.86
Tilt 13	2.59	3.76	4.91	6.40	7.30	7.71	7.40	6.79	5.70	4.47	3.15	2.41	5.22
Tilt 18	2.76	3.94	5.04	6.45	7.25	7.61	7.32	6.80	5.82	4.66	3.36	2.58	5.30
Tilt 23	2.91	4.11	5.14	6.47	7.16	7.46	7.20	6.77	5.91	4.83	3.54	2.74	5.35
Tilt 28	3.05	4.24	5.22	6.44	7.02	7.27	7.04	6.70	5.96	4.96	3.70	2.88	5.37
Tilt 33	3.16	4.36	5.26	6.38	6.85	7.03	6.84	6.60	5.98	5.07	3.83	3.00	5.36
Tilt 38	3.26	4.44	5.28	6.28	6.64	6.76	6.60	6.45	5.96	5.14	3.95	3.10	5.32
Tilt 43	3.33	4.50	5.26	6.15	6.39	6.45	6.32	6.27	5.90	5.19	4.04	3.19	5.25
Tilt 48	3.39	4.53	5.21	5.98	6.10	6.11	6.01	6.05	5.81	5.20	4.10	3.25	5.15
Tilt 53	3.42	4.54	5.14	5.77	5.79	5.73	5.67	5.80	5.69	5.18	4.14	3.30	5.01
Tilt 58	3.44	4.51	5.03	5.54	5.44	5.34	5.31	5.52	5.53	5.13	4.15	3.32	4.86
Tilt 63	3.43	4.46	4.89	5.28	5.09	4.94	4.93	5.22	5.35	5.05	4.13	3.33	4.67
Tilt 90	3.03	3.72	3.72	3.50	2.99	2.72	2.80	3.29	3.86	4.12	3.62	2.99	3.36
Optimum	3.44	4.54	5.28	6.47	7.30	7.77	7.40	6.80	5.98	5.20	4.15	3.33	5.64
Angle	58	53	38	23	13	0	0	18	33	48	58	63	33

Table 4. Average Tilted Surface Radiation using Perez Non-Isotropic Diffuse Method with Extended Page Horizontal Diffuse (kWhr/m^2/day).
Sacramento, CA, Latitude 38.5^o N, Longitude 121.5^o W, Tilt toward South.

Month	**1**	**2**	**3**	**4**	**5**	**6**	**7**	**8**	**9**	**10**	**11**	**12**	**Avg**
SSE HRZ	2.11	3.26	4.48	6.13	7.27	7.83	7.45	6.61	5.32	3.88	2.58	1.91	4.90
PAG DIF	0.96	1.18	1.52	1.64	1.69	1.65	1.72	1.63	1.48	1.24	1.00	0.87	1.38
PAG DNR	3.12	4.68	5.56	7.40	8.68	9.46	8.83	7.98	6.82	5.58	4.07	3.00	6.26
Tilt 0	2.09	3.17	4.44	6.10	7.23	7.77	7.40	6.59	5.24	3.85	2.55	1.90	4.86
Tilt 13	2.78	3.96	5.20	6.64	7.46	7.82	7.54	7.00	5.99	4.80	3.34	2.59	5.43
Tilt 18	3.01	4.22	5.44	6.77	7.45	7.75	7.49	7.07	6.21	5.10	3.61	2.82	5.58
Tilt 23	3.23	4.45	5.63	6.85	7.39	7.62	7.40	7.09	6.38	5.37	3.85	3.04	5.69
Tilt 28	3.42	4.65	5.79	6.88	7.28	7.43	7.25	7.06	6.51	5.60	4.07	3.24	5.77
Tilt 33	3.59	4.82	5.91	6.87	7.12	7.20	7.06	6.99	6.60	5.80	4.26	3.41	5.80
Tilt 38	3.73	4.96	5.99	6.80	6.91	6.91	6.81	6.86	6.63	5.95	4.42	3.57	5.80
Tilt 43	3.85	5.06	6.02	6.69	6.66	6.59	6.53	6.70	6.63	6.06	4.55	3.69	5.75
Tilt 48	3.95	5.13	6.02	6.54	6.36	6.23	6.20	6.48	6.57	6.13	4.65	3.80	5.67
Tilt 53	4.01	5.16	5.97	6.34	6.04	5.85	5.86	6.23	6.47	6.16	4.71	3.88	5.56
Tilt 58	4.05	5.16	5.88	6.10	5.69	5.43	5.47	5.94	6.33	6.14	4.75	3.93	5.41
Tilt 63	4.07	5.12	5.75	5.82	5.29	4.98	5.05	5.62	6.14	6.08	4.75	3.95	5.22
Tilt 90	3.66	4.33	4.40	3.73	2.81	2.38	2.54	3.34	4.45	5.05	4.20	3.62	3.71
Optimum	4.07	5.16	6.02	6.88	7.46	7.82	7.54	7.09	6.63	6.16	4.75	3.95	6.13
Angle	63	53	43	28	13	13	13	23	38	53	63	63	38

Table 5. Average Tilted Surface Radiation using Perez Non-Isotropic Diffuse Method with Erbs et al. Diffuse (kWhr/m^2/day).
Sacramento, CA, Latitude 38.5^o N, Longitude 121.5^o W, Tilt toward South.

Month	**1**	**2**	**3**	**4**	**5**	**6**	**7**	**8**	**9**	**10**	**11**	**12**	**Avg**
SSE HRZ	2.11	3.26	4.48	6.13	7.27	7.83	7.45	6.61	5.32	3.88	2.58	1.91	4.90
RET DIF	0.88	1.11	1.63	1.90	2.06	2.10	2.11	1.95	1.70	1.36	0.93	0.80	1.54
RET DNR	3.17	4.31	5.03	6.87	7.65	8.11	7.68	7.23	5.92	5.22	3.97	3.10	5.69
Tilt 0	2.09	3.17	4.44	6.10	7.23	7.77	7.40	6.59	5.24	3.85	2.55	1.90	4.86
Tilt 13	2.80	3.99	5.17	6.64	7.48	7.86	7.57	7.02	5.99	4.75	3.37	2.61	5.44
Tilt 18	3.04	4.26	5.40	6.77	7.49	7.79	7.54	7.09	6.20	5.04	3.64	2.85	5.59
Tilt 23	3.26	4.50	5.59	6.85	7.44	7.68	7.45	7.12	6.37	5.29	3.90	3.07	5.71
Tilt 28	3.45	4.71	5.73	6.88	7.34	7.50	7.32	7.11	6.50	5.51	4.12	3.28	5.79
Tilt 33	3.63	4.89	5.85	6.87	7.19	7.28	7.13	7.04	6.59	5.70	4.32	3.46	5.83
Tilt 38	3.78	5.03	5.92	6.81	6.99	7.01	6.90	6.92	6.62	5.84	4.49	3.62	5.83
Tilt 43	3.90	5.14	5.95	6.70	6.75	6.70	6.63	6.76	6.62	5.94	4.62	3.75	5.79
Tilt 48	4.00	5.21	5.94	6.55	6.47	6.34	6.31	6.56	6.56	6.00	4.73	3.86	5.71
Tilt 53	4.07	5.25	5.88	6.36	6.14	5.95	5.95	6.31	6.47	6.02	4.80	3.94	5.59
Tilt 58	4.11	5.25	5.79	6.12	5.79	5.54	5.57	6.02	6.32	6.00	4.84	3.99	5.45
Tilt 63	4.13	5.22	5.66	5.84	5.40	5.09	5.16	5.70	6.14	5.94	4.84	4.02	5.26
Tilt 90	3.72	4.42	4.33	3.79	2.94	2.51	2.66	3.44	4.46	4.92	4.29	3.69	3.77
Optimum	4.13	5.25	5.95	6.88	7.49	7.86	7.57	7.12	6.62	6.02	4.84	4.02	6.15
Angle	63	58	43	28	18	13	13	23	38	53	63	63	39

Table 6. Equivalent Sun Hours Tilted Surface Radiation using RETScreen Method (kWhr/m^2/day).
Sacramento, CA, Latitude 38.5^o N, Longitude 121.5^o W, Tilt toward South.

Month	**1**	**2**	**3**	**4**	**5**	**6**	**7**	**8**	**9**	**10**	**11**	**12**	**Avg**
SSE HRZ	1.70	2.71	3.74	5.41	6.46	7.33	6.94	6.34	4.92	3.50	2.00	1.40	4.37
RET DIF	0.89	1.17	1.69	2.03	2.25	2.24	2.24	2.02	1.77	1.40	0.97	0.80	1.62
RET DNR	2.05	3.07	3.56	5.42	6.14	7.18	6.73	6.68	5.12	4.29	2.43	1.61	4.52
Tilt 0	1.69	2.64	3.70	5.39	6.43	7.27	6.90	6.32	4.85	3.48	1.98	1.40	4.34
Tilt 13	2.01	3.05	4.04	5.62	6.48	7.22	6.89	6.51	5.25	3.98	2.35	1.66	4.59
Tilt 18	2.11	3.18	4.13	5.66	6.43	7.12	6.82	6.51	5.35	4.14	2.47	1.74	4.64
Tilt 23	2.21	3.29	4.19	5.66	6.35	6.99	6.71	6.48	5.42	4.27	2.57	1.82	4.67
Tilt 28	2.29	3.39	4.24	5.64	6.24	6.81	6.57	6.42	5.46	4.38	2.66	1.89	4.66
Tilt 33	2.36	3.46	4.26	5.58	6.09	6.60	6.38	6.32	5.47	4.46	2.74	1.95	4.64
Tilt 38	2.42	3.51	4.26	5.49	5.91	6.35	6.16	6.18	5.44	4.52	2.80	1.99	4.59
Tilt 43	2.46	3.55	4.24	5.37	5.69	6.07	5.91	6.00	5.39	4.55	2.85	2.03	4.51
Tilt 48	2.49	3.56	4.19	5.23	5.45	5.76	5.63	5.80	5.31	4.55	2.88	2.05	4.41
Tilt 53	2.50	3.55	4.12	5.05	5.18	5.41	5.32	5.56	5.19	4.53	2.89	2.06	4.28
Tilt 58	2.50	3.52	4.03	4.85	4.88	5.04	4.98	5.29	5.05	4.48	2.88	2.07	4.13
Tilt 63	2.48	3.47	3.92	4.62	4.56	4.67	4.63	5.00	4.88	4.40	2.86	2.06	3.96
Tilt 90	2.16	2.88	2.98	3.11	2.77	2.65	2.70	3.17	3.53	3.58	2.47	1.81	2.82
Optimum	2.50	3.56	4.26	5.66	6.48	7.27	6.90	6.51	5.47	4.55	2.89	2.07	4.84
Angle	53	48	33	23	13	0	0	18	33	48	53	58	31

Table 7. Equivalent Sun Hours Tilted Surface Radiation using Perez Non-Isotropic Diffuse Method with Extended Page Horizontal Diffuse (kWhr/m^2/day).
Sacramento, CA, Latitude 38.5^o N, Longitude 121.5^o W, Tilt toward South.

Month	**1**	**2**	**3**	**4**	**5**	**6**	**7**	**8**	**9**	**10**	**11**	**12**	**Avg**
SSE HRZ	1.70	2.71	3.74	5.41	6.46	7.33	6.94	6.34	4.92	3.50	2.00	1.40	4.37
PAG DIF	0.95	1.27	1.68	1.91	2.05	1.92	1.96	1.76	1.64	1.35	1.05	0.84	1.53
PAG DNR	2.03	3.23	3.87	5.77	6.85	8.29	7.66	7.34	5.83	4.54	2.45	1.61	4.96
Tilt 0	1.69	2.64	3.70	5.39	6.43	7.27	6.90	6.32	4.85	3.48	1.98	1.40	4.34
Tilt 13	2.10	3.21	4.26	5.86	6.66	7.35	7.05	6.72	5.52	4.24	2.43	1.75	4.76
Tilt 18	2.23	3.40	4.43	5.97	6.66	7.29	7.02	6.80	5.71	4.49	2.58	1.86	4.87
Tilt 23	2.36	3.56	4.57	6.04	6.63	7.18	6.94	6.82	5.86	4.70	2.72	1.97	4.95
Tilt 28	2.46	3.71	4.68	6.07	6.54	7.02	6.82	6.80	5.98	4.89	2.84	2.07	4.99
Tilt 33	2.56	3.83	4.76	6.06	6.41	6.81	6.65	6.73	6.05	5.04	2.94	2.15	5.00
Tilt 38	2.64	3.92	4.80	6.01	6.24	6.55	6.43	6.62	6.08	5.16	3.02	2.22	4.97
Tilt 43	2.70	3.99	4.82	5.92	6.03	6.26	6.17	6.46	6.07	5.24	3.08	2.28	4.92
Tilt 48	2.74	4.03	4.80	5.79	5.79	5.92	5.88	6.27	6.02	5.29	3.12	2.32	4.83
Tilt 53	2.77	4.04	4.76	5.62	5.50	5.56	5.55	6.02	5.93	5.30	3.15	2.35	4.71
Tilt 58	2.78	4.03	4.68	5.42	5.18	5.18	5.20	5.75	5.80	5.28	3.15	2.36	4.57
Tilt 63	2.77	3.99	4.57	5.17	4.84	4.76	4.81	5.44	5.63	5.22	3.13	2.36	4.39
Tilt 90	2.44	3.36	3.49	3.38	2.69	2.34	2.48	3.27	4.09	4.31	2.71	2.11	3.05
Optimum	2.78	4.04	4.82	6.07	6.66	7.35	7.05	6.82	6.08	5.30	3.15	2.36	5.21
Angle	58	53	43	28	18	13	13	23	38	53	58	58	38

Table 8. Equivalent Sun Hours Tilted Surface Radiation using Perez Non-Isotropic Diffuse Method with Erbs et al. Horizontal Diffuse (kWhr/m^2/day).
Sacramento, CA, Latitude 38.5^o N, Longitude 121.5^o W, Tilt toward South.

Month	**1**	**2**	**3**	**4**	**5**	**6**	**7**	**8**	**9**	**10**	**11**	**12**	**Avg**
SSE HRZ	1.70	2.71	3.74	5.41	6.46	7.33	6.94	6.34	4.92	3.50	2.00	1.40	4.37
RET DIF	0.89	1.17	1.69	2.03	2.25	2.24	2.24	2.02	1.77	1.40	0.97	0.80	1.62
RET DNR	2.05	3.07	3.56	5.42	6.14	7.18	6.73	6.68	5.12	4.29	2.43	1.61	4.52
Tilt 0	1.69	2.64	3.70	5.39	6.43	7.27	6.90	6.32	4.85	3.48	1.98	1.40	4.34
Tilt 13	2.13	3.26	4.26	5.85	6.66	7.38	7.06	6.73	5.50	4.24	2.54	1.76	4.78
Tilt 18	2.28	3.47	4.43	5.96	6.67	7.32	7.04	6.80	5.69	4.48	2.72	1.89	4.89
Tilt 23	2.41	3.65	4.57	6.02	6.63	7.22	6.97	6.83	5.83	4.69	2.89	2.00	4.98
Tilt 28	2.53	3.81	4.68	6.05	6.55	7.07	6.85	6.81	5.94	4.88	3.04	2.10	5.03
Tilt 33	2.64	3.94	4.75	6.04	6.43	6.87	6.69	6.75	6.01	5.03	3.18	2.19	5.04
Tilt 38	2.72	4.05	4.80	5.98	6.26	6.62	6.48	6.64	6.04	5.14	3.29	2.26	5.02
Tilt 43	2.79	4.13	4.82	5.89	6.06	6.34	6.23	6.49	6.03	5.23	3.37	2.32	4.97
Tilt 48	2.85	4.18	4.80	5.76	5.81	6.01	5.94	6.29	5.98	5.27	3.44	2.37	4.89
Tilt 53	2.88	4.20	4.75	5.60	5.53	5.65	5.61	6.06	5.88	5.29	3.48	2.40	4.78
Tilt 58	2.89	4.20	4.68	5.39	5.21	5.26	5.25	5.78	5.75	5.26	3.50	2.41	4.63
Tilt 63	2.89	4.16	4.57	5.15	4.87	4.85	4.87	5.48	5.58	5.20	3.49	2.41	4.46
Tilt 90	2.56	3.52	3.49	3.38	2.74	2.45	2.58	3.34	4.06	4.30	3.07	2.16	3.14
Optimum	2.89	4.20	4.82	6.05	6.67	7.38	7.06	6.83	6.04	5.29	3.50	2.41	5.26
Angle	58	53	43	28	18	13	13	23	38	53	58	63	38

Table 9. Peak Sun Hours Tilted Surface Radiation using RETScreen Method (kWhr/m^2/day).
Sacramento, CA, Latitude 38.5^o N, Longitude 121.5^o W, Tilt toward South.

Month	**1**	**2**	**3**	**4**	**5**	**6**	**7**	**8**	**9**	**10**	**11**	**12**	**Avg**
SSE HRZ	2.50	3.94	5.57	6.52	7.85	8.34	7.80	6.89	5.62	4.12	3.08	2.27	5.37
RET DIF	0.83	0.95	1.35	1.79	1.86	1.90	1.99	1.87	1.62	1.31	0.84	0.76	1.42
RET DNR	4.34	6.01	7.56	7.72	8.84	9.14	8.37	7.82	6.55	5.84	5.44	4.27	6.83
Tilt 0	2.48	3.83	5.51	6.49	7.81	8.28	7.75	6.86	5.54	4.09	3.04	2.26	5.33
Tilt 13	3.17	4.65	6.23	6.83	7.89	8.21	7.75	7.09	6.05	4.78	3.88	2.96	5.79
Tilt 18	3.40	4.92	6.44	6.89	7.83	8.10	7.67	7.10	6.18	5.00	4.16	3.20	5.91
Tilt 23	3.61	5.15	6.60	6.90	7.73	7.93	7.54	7.07	6.28	5.18	4.41	3.42	5.99
Tilt 28	3.80	5.35	6.73	6.88	7.59	7.73	7.37	7.00	6.34	5.34	4.63	3.62	6.03
Tilt 33	3.96	5.52	6.82	6.82	7.39	7.47	7.15	6.89	6.36	5.46	4.83	3.79	6.04
Tilt 38	4.10	5.65	6.86	6.71	7.16	7.17	6.90	6.73	6.35	5.55	4.99	3.94	6.01
Tilt 43	4.21	5.75	6.86	6.57	6.88	6.84	6.60	6.54	6.29	5.60	5.12	4.07	5.94
Tilt 48	4.30	5.80	6.82	6.39	6.57	6.46	6.27	6.31	6.20	5.62	5.22	4.16	5.84
Tilt 53	4.36	5.82	6.73	6.17	6.21	6.06	5.91	6.05	6.07	5.61	5.29	4.23	5.71
Tilt 58	4.39	5.81	6.60	5.92	5.86	5.65	5.53	5.76	5.91	5.56	5.32	4.28	5.55
Tilt 63	4.39	5.75	6.43	5.64	5.46	5.21	5.14	5.44	5.71	5.48	5.31	4.29	5.35
Tilt 90	3.92	4.83	4.89	3.71	3.12	2.78	2.86	3.40	4.11	4.47	4.69	3.90	3.89
Optimum	4.39	5.82	6.86	6.90	7.89	8.28	7.75	7.10	6.36	5.62	5.32	4.29	6.38
Angle	63	53	38	23	13	0	0	18	33	48	58	63	34

Table 10. Peak Sun Hours Tilted Surface Radiation using Perez Non-Isotropic Diffuse Method with Extended Page Horizontal Diffuse (kWhr/m^2/day).
Sacramento, CA, Latitude 38.5^o N, Longitude 121.5^o W, Tilt toward South.

Month	**1**	**2**	**3**	**4**	**5**	**6**	**7**	**8**	**9**	**10**	**11**	**12**	**Avg**
SSE HRZ	2.50	3.94	5.57	6.52	7.85	8.34	7.80	6.89	5.62	4.12	3.08	2.27	5.37
PAG DIF	0.88	0.90	0.99	1.44	1.34	1.33	1.52	1.48	1.33	1.14	0.83	0.80	1.17
PAG DNR	4.39	6.84	8.59	8.38	10.12	10.73	9.68	8.67	7.61	6.29	5.80	4.24	7.61
Tilt 0	2.48	3.83	5.51	6.49	7.81	8.28	7.75	6.86	5.54	4.09	3.04	2.26	5.33
Tilt 13	3.39	4.90	6.50	7.05	8.02	8.30	7.87	7.28	6.32	5.11	4.13	3.18	6.00
Tilt 18	3.70	5.25	6.80	7.18	8.00	8.21	7.82	7.35	6.55	5.44	4.50	3.50	6.19
Tilt 23	3.99	5.57	7.05	7.25	7.93	8.06	7.71	7.36	6.73	5.74	4.84	3.79	6.33
Tilt 28	4.25	5.84	7.25	7.28	7.80	7.86	7.55	7.33	6.86	5.99	5.14	4.06	6.43
Tilt 33	4.48	6.08	7.40	7.26	7.62	7.59	7.34	7.25	6.95	6.20	5.41	4.30	6.49
Tilt 38	4.68	6.27	7.49	7.18	7.38	7.28	7.08	7.11	6.98	6.37	5.64	4.51	6.50
Tilt 43	4.84	6.42	7.54	7.06	7.10	6.92	6.78	6.93	6.97	6.49	5.83	4.68	6.46
Tilt 48	4.98	6.52	7.53	6.89	6.78	6.54	6.43	6.71	6.91	6.57	5.97	4.83	6.39
Tilt 53	5.07	6.57	7.47	6.67	6.43	6.13	6.07	6.44	6.80	6.60	6.08	4.94	6.27
Tilt 58	5.14	6.58	7.35	6.42	6.04	5.68	5.66	6.14	6.65	6.58	6.14	5.02	6.12
Tilt 63	5.16	6.55	7.18	6.12	5.60	5.19	5.22	5.80	6.45	6.52	6.15	5.06	5.92
Tilt 90	4.68	5.56	5.45	3.88	2.89	2.38	2.56	3.42	4.64	5.41	5.49	4.67	4.25
Optimum	5.16	6.58	7.54	7.28	8.02	8.30	7.87	7.36	6.98	6.60	6.15	5.06	6.91
Angle	63	58	43	28	13	13	13	23	38	53	63	63	39

Table 11. Peak Sun Hours Tilted Surface Radiation using Perez Non-Isotropic Diffuse Method with RETScreen Horizontal Diffuse (kWhr/m^2/day).
Sacramento, CA, Latitude 38.5^o N, Longitude 121.5^o W, Tilt toward South.

Month	**1**	**2**	**3**	**4**	**5**	**6**	**7**	**8**	**9**	**10**	**11**	**12**	**Avg**
SSE HRZ	2.50	3.94	5.57	6.52	7.85	8.34	7.80	6.89	5.62	4.12	3.08	2.27	5.37
RET DIF	0.83	0.95	1.35	1.79	1.86	1.90	1.99	1.87	1.62	1.31	0.84	0.76	1.42
RET DNR	4.34	6.01	7.56	7.72	8.84	9.14	8.37	7.82	6.55	5.84	5.44	4.27	6.83
Tilt 0	2.48	3.83	5.51	6.49	7.81	8.28	7.75	6.86	5.54	4.09	3.04	2.26	5.33
Tilt 13	3.44	4.90	6.50	7.07	8.05	8.34	7.91	7.30	6.33	5.10	4.13	3.22	6.02
Tilt 18	3.76	5.25	6.80	7.21	8.05	8.26	7.87	7.38	6.56	5.43	4.50	3.56	6.22
Tilt 23	4.06	5.56	7.05	7.29	7.98	8.13	7.77	7.41	6.74	5.72	4.84	3.86	6.37
Tilt 28	4.34	5.84	7.25	7.33	7.86	7.93	7.63	7.38	6.88	5.97	5.14	4.15	6.48
Tilt 33	4.58	6.07	7.40	7.31	7.69	7.69	7.43	7.31	6.97	6.18	5.41	4.40	6.54
Tilt 38	4.79	6.26	7.50	7.24	7.47	7.39	7.18	7.18	7.01	6.35	5.64	4.62	6.55
Tilt 43	4.97	6.41	7.55	7.13	7.20	7.05	6.88	7.01	7.00	6.47	5.83	4.81	6.53
Tilt 48	5.11	6.51	7.54	6.96	6.88	6.66	6.55	6.80	6.95	6.55	5.97	4.96	6.45
Tilt 53	5.22	6.57	7.48	6.75	6.53	6.26	6.18	6.53	6.84	6.58	6.08	5.08	6.34
Tilt 58	5.28	6.58	7.37	6.50	6.15	5.81	5.78	6.24	6.69	6.56	6.14	5.17	6.19
Tilt 63	5.32	6.54	7.20	6.20	5.72	5.33	5.34	5.90	6.49	6.50	6.15	5.22	5.99
Tilt 90	4.84	5.56	5.48	3.98	3.05	2.57	2.71	3.53	4.71	5.40	5.49	4.84	4.35
Optimum	5.32	6.58	7.55	7.33	8.05	8.34	7.91	7.41	7.01	6.58	6.15	5.22	6.95
Angle	63	58	43	28	13	13	13	23	38	53	63	63	39

Table 12. Wind Velocity V10/V50 Ratio for Various Vegetation Types.

Northern hemisphere month	1	2	3	4	5	6	7	8	9	10	11	12
35-m broadleaf-evergreen trees (70%)	0.47	0.47	0.47	0.47	0.47	0.47	0.47	0.47	0.47	0.47	0.47	0.47
20-m broadleaf-deciduous trees (75%)	0.58	0.57	0.56	0.55	0.53	0.51	0.49	0.51	0.53	0.55	0.56	0.57
20-m broadleaf & needleleaf trees (75%)	0.44	0.47	0.50	0.52	0.53	0.54	0.54	0.52	0.50	0.48	0.46	0.45
17-m needleleaf-evergreen trees (75%)	0.50	0.53	0.56	0.58	0.57	0.56	0.55	0.55	0.55	0.54	0.53	0.52
14-m needleleaf-deciduous trees (50%)	0.52	0.53	0.55	0.57	0.57	0.58	0.58	0.54	0.51	0.49	0.49	0.50
18-m broadleaf trees (30%)/groundcover	0.52	0.52	0.52	0.52	0.52	0.52	0.52	0.52	0.52	0.52	0.52	0.52
0.6-m perennial groundcover (100%)	0.65	0.65	0.65	0.65	0.65	0.65	0.65	0.65	0.65	0.65	0.65	0.65
0.5-m broadleaf (variable %)/groundcover	0.65	0.65	0.65	0.65	0.65	0.65	0.65	0.65	0.65	0.65	0.65	0.65
0.5-m broadleaf shrubs (10%)/bare soil	0.65	0.65	0.65	0.65	0.65	0.65	0.65	0.65	0.65	0.65	0.65	0.65
0.6-m shrubs (variable %)/groundcover	0.65	0.65	0.65	0.65	0.65	0.65	0.65	0.65	0.65	0.65	0.65	0.65
Rough bare soil	0.70	0.70	0.70	0.70	0.70	0.70	0.70	0.70	0.70	0.70	0.70	0.70
Crop: 20-m broadleaf-deciduous trees (10%) & wheat	0.64	0.62	0.69	0.57	0.57	0.57	0.57	0.57	0.57	0.59	0.61	0.63
Rough glacial snow/ice	0.57	0.59	0.62	0.64	0.64	0.64	0.64	0.64	0.62	0.59	0.58	0.57
Smooth sea ice	0.75	0.78	0.83	0.86	0.86	0.86	0.86	0.82	0.78	0.74	0.74	0.74
Open water	0.85	0.85	0.85	0.85	0.85	0.85	0.85	0.85	0.85	0.85	0.85	0.85
"Airport": flat ice/snow	0.85	0.85	0.85	0.85	0.85	0.85	0.85	0.85	0.85	0.85	0.85	0.85
"Airport": flat rough grass	0.79	0.79	0.79	0.79	0.79	0.79	0.79	0.79	0.79	0.79	0.79	0.79

Note: 10-m and 50-m heights are above soil, water, or ice surfaces, not above the "effective" surface near the tops of vegetation.

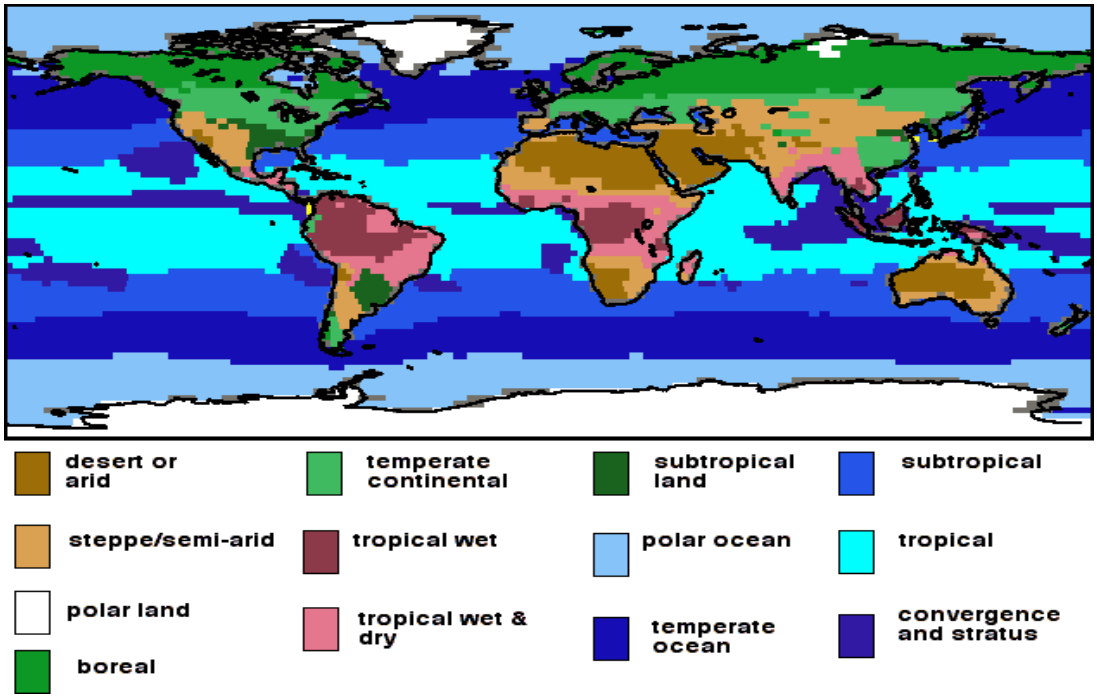

(a) Map of various climate regions.

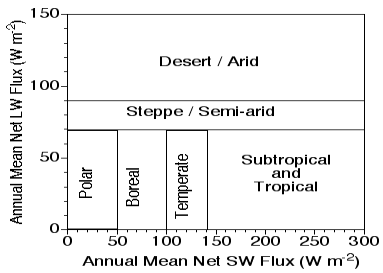

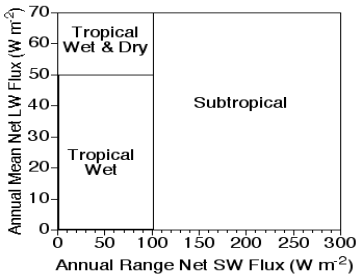

(b) Criteria for classification of land regions. (c) Criteria for classification of tropical and subtropical regions.

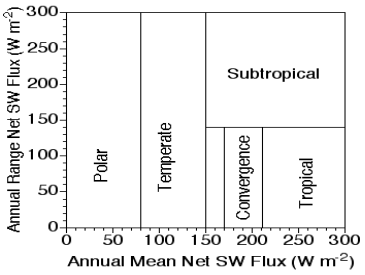

(d) Criteria for classification of ocean regions.

Figure 1. Climate classification based on radiation absorbed into the Earth's surface (net SW and LW).

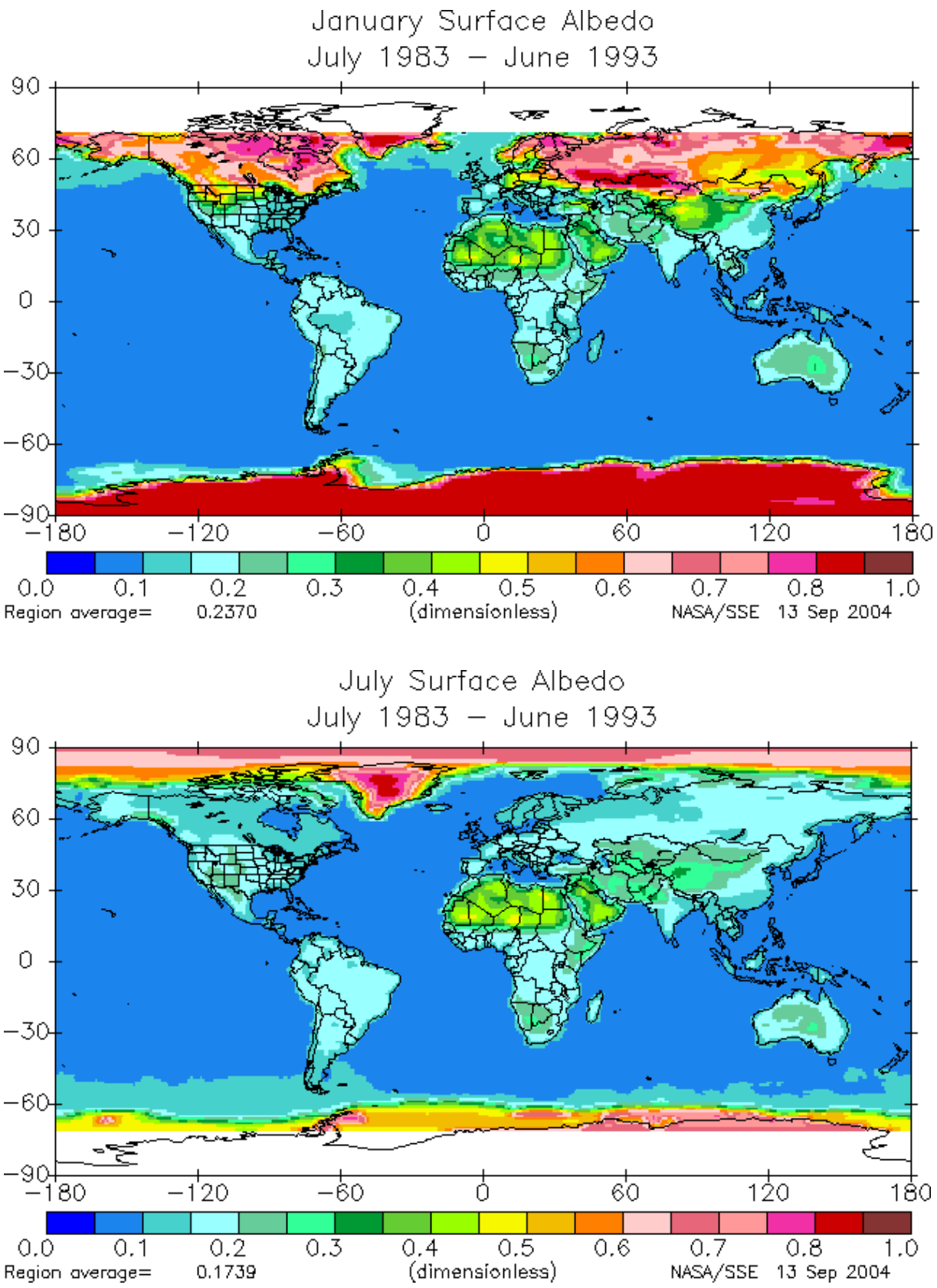

Figure 2. SSE satellite-derived surface albedo.

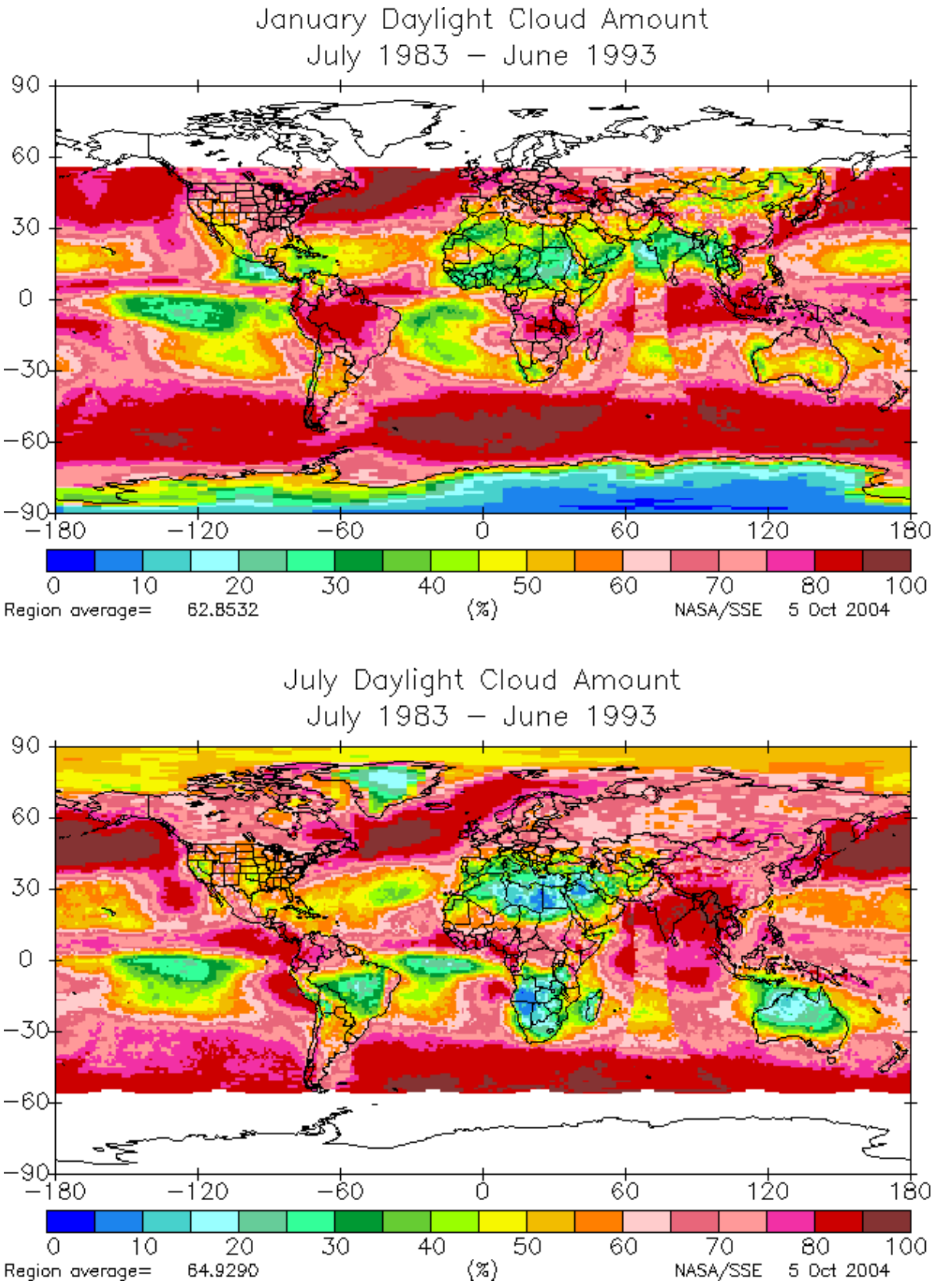

Figure 3. SSE satellite-derived daylight cloud amount.

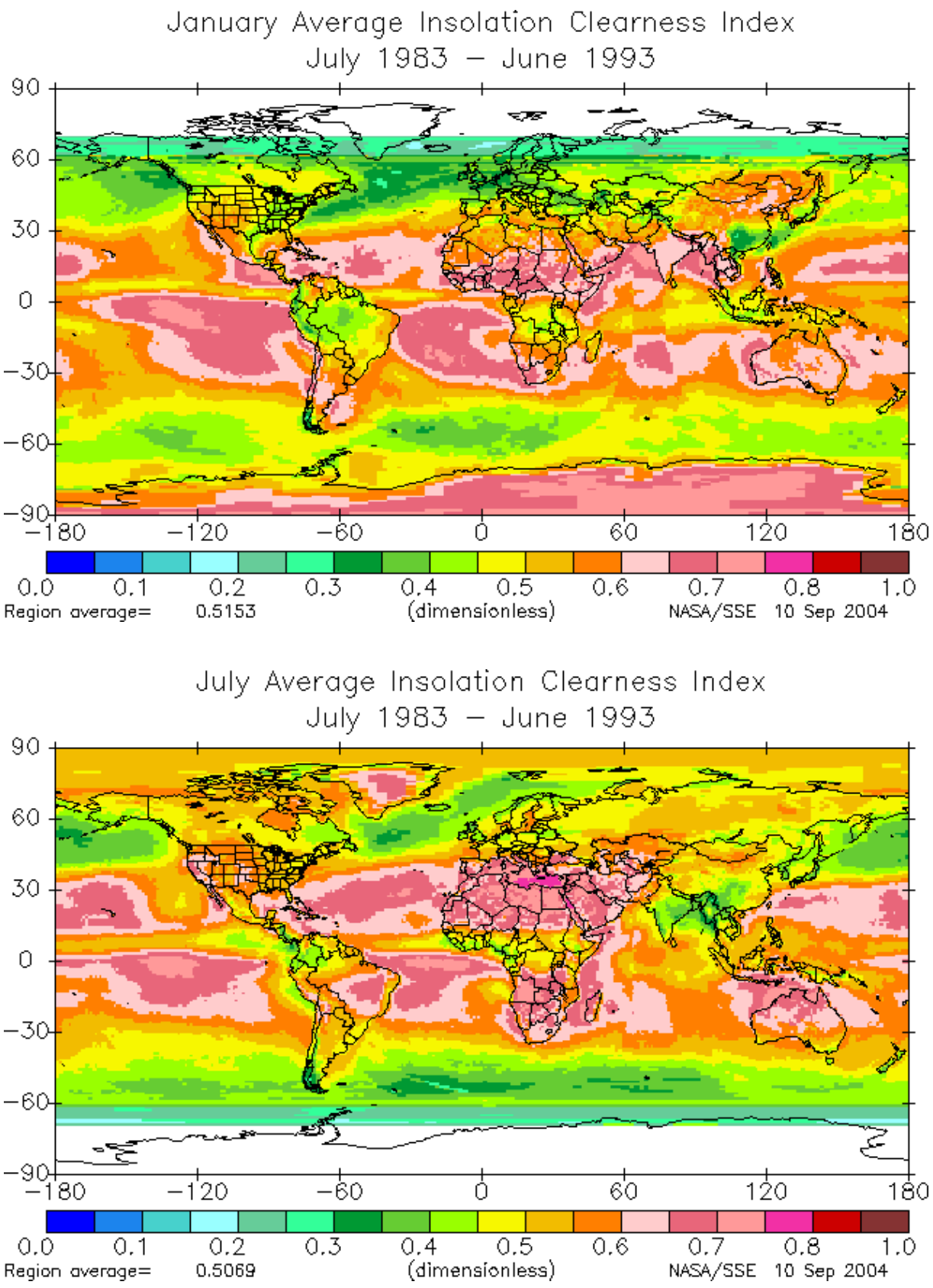

Figure 4. SSE-derived monthly average insolation clearness index.

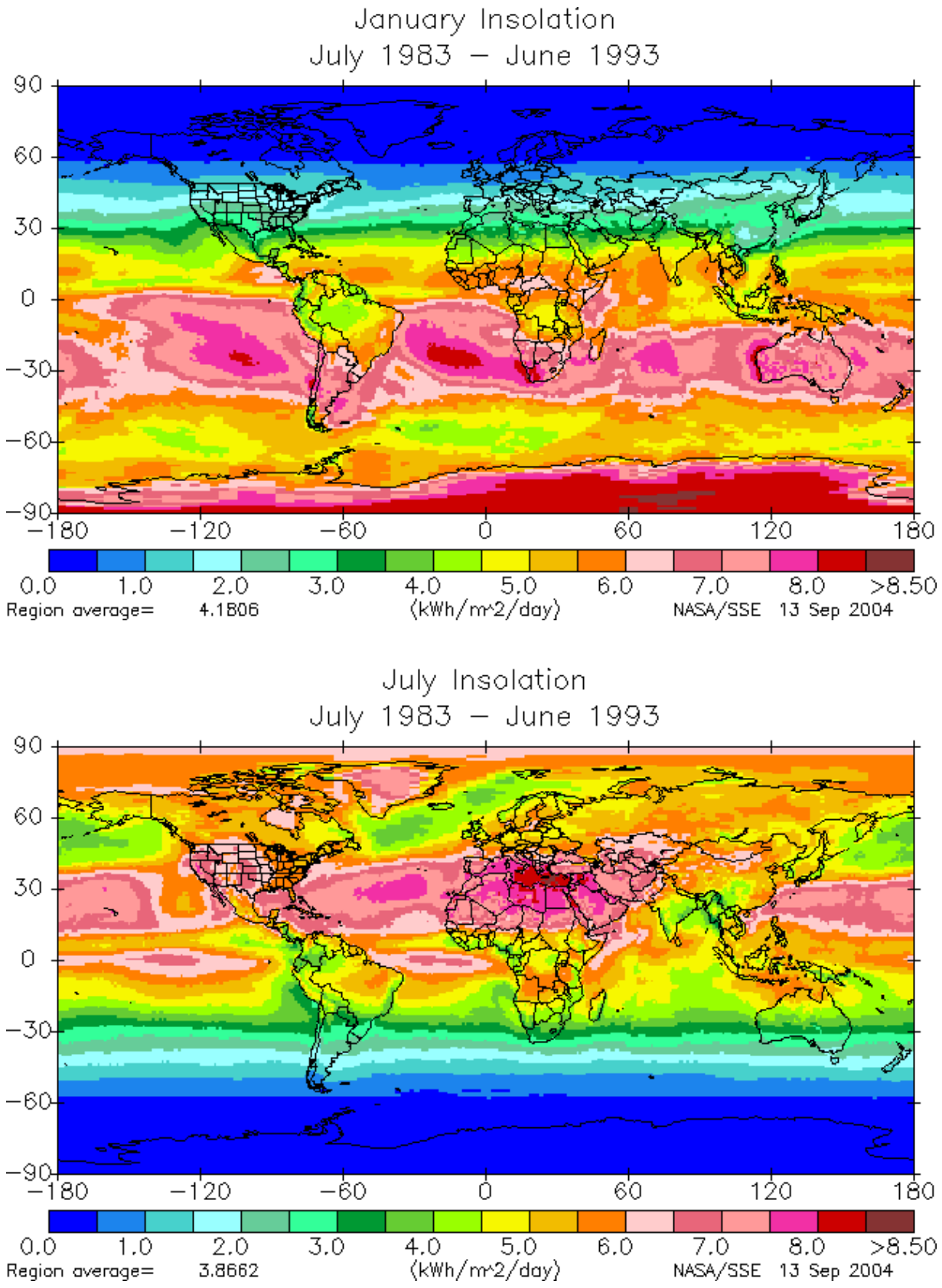

Figure 5. SSE-derived monthly average insolation.

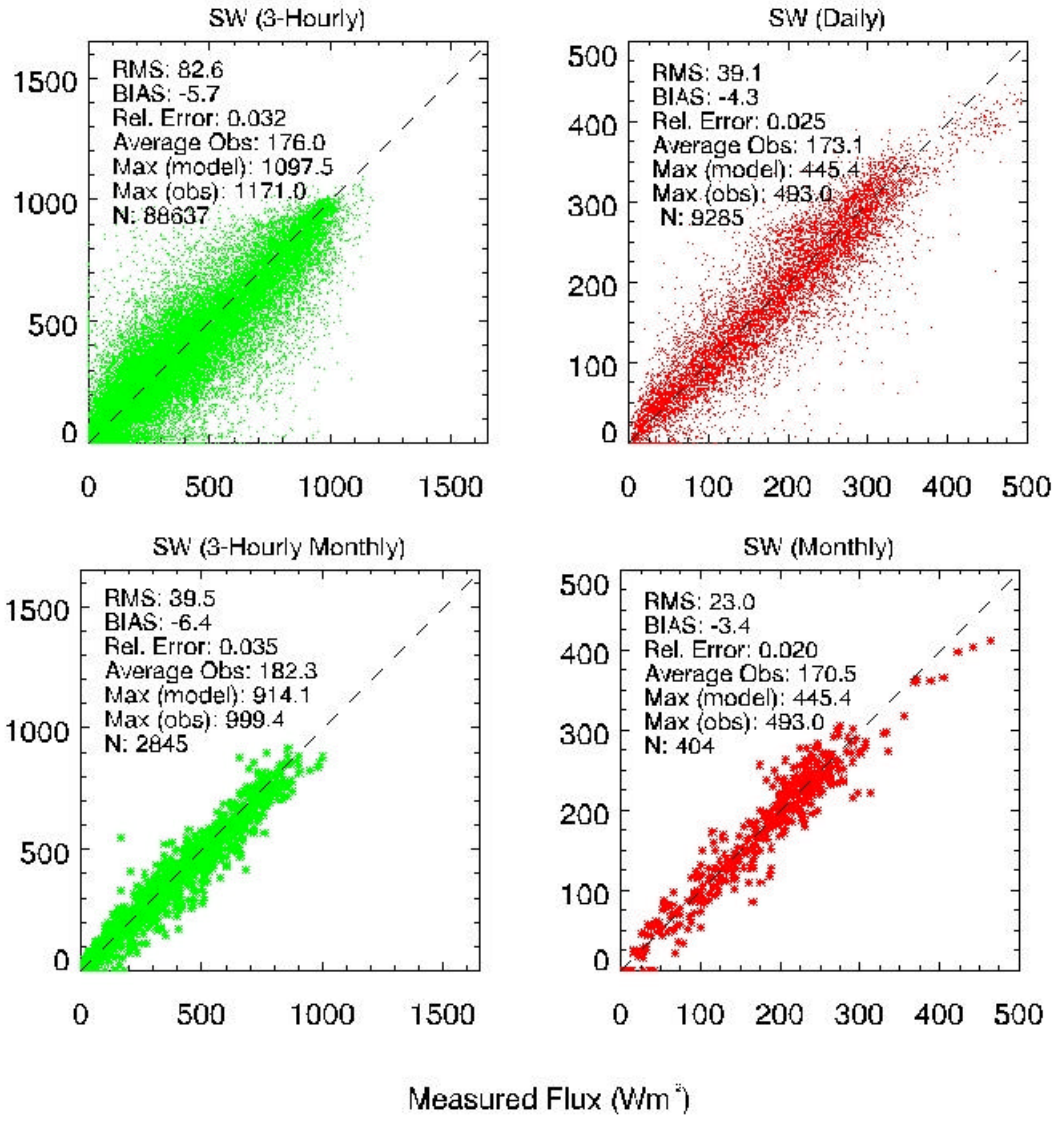

Figure 6. Insolation accuracy for 1992-1995 high-quality BSRN sites available from the Swiss Federal Institute of Technology.

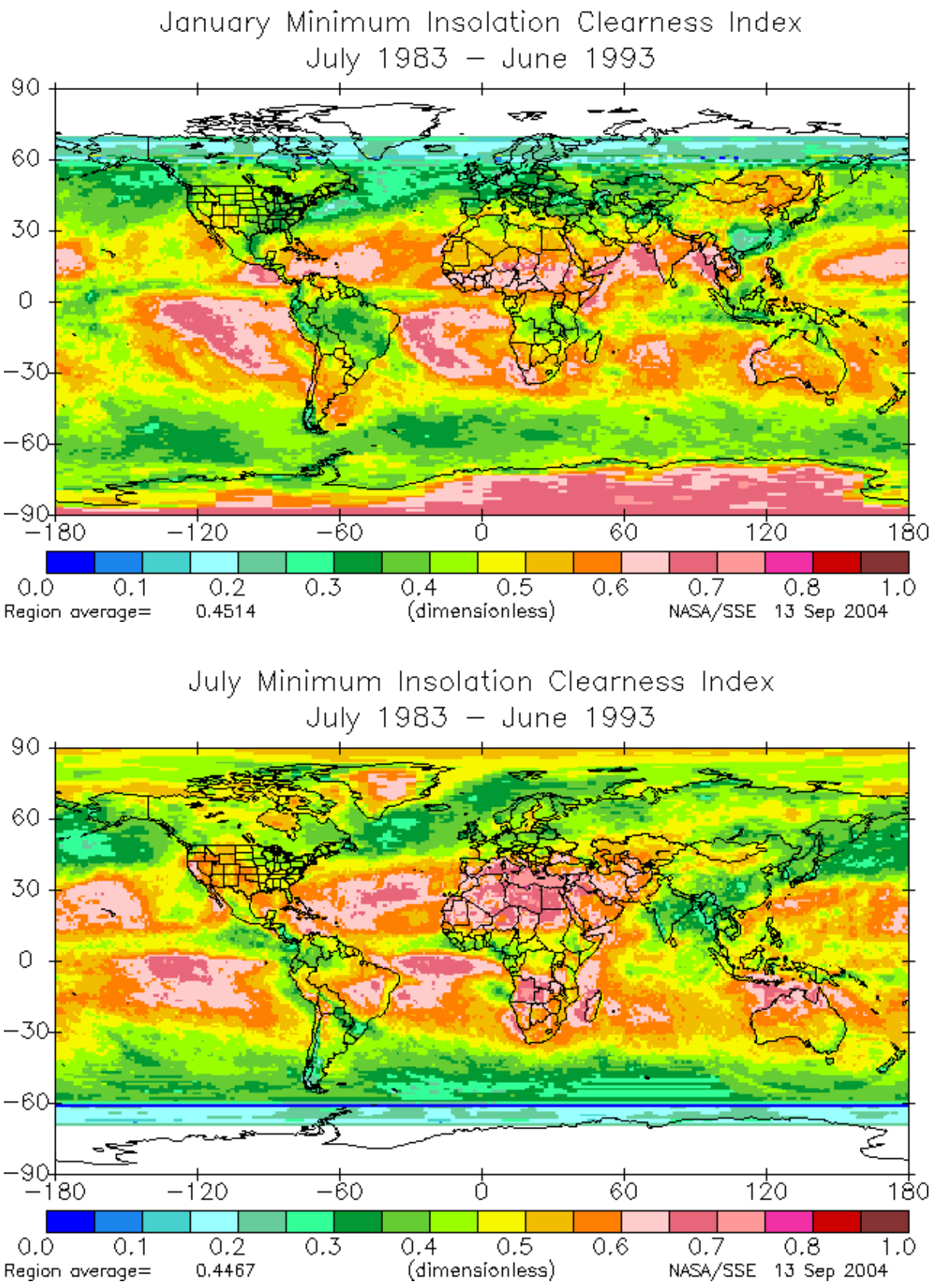

Figure 7. SSE-derived monthly minimum insolation clearness index.

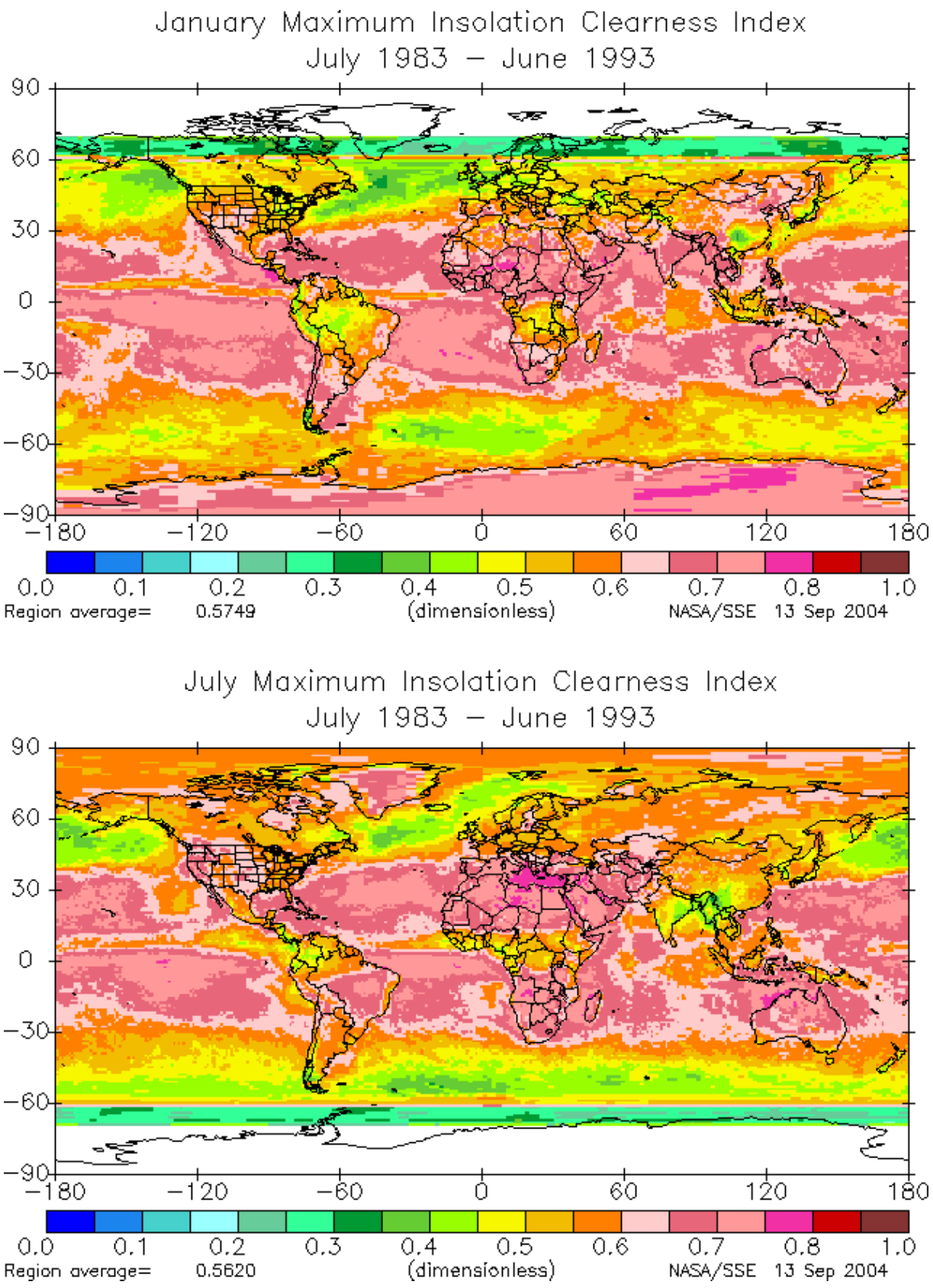

Figure 8. SSE-derived monthly maximum insolation clearness index.

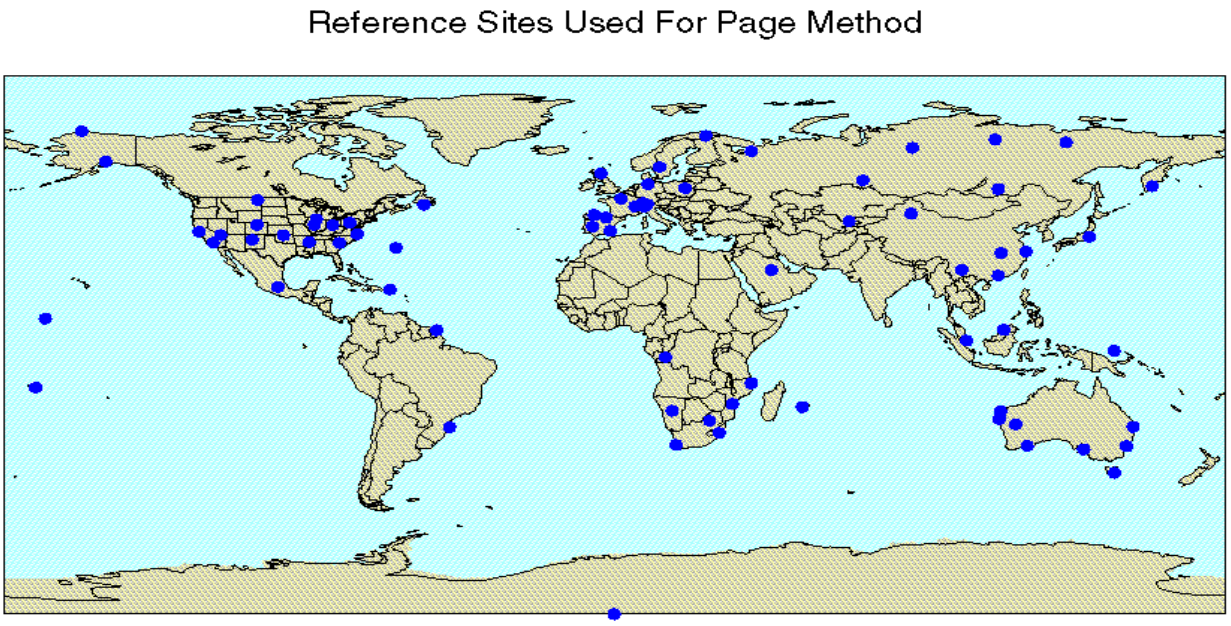

Figure 9. Historical and recent reference sites used to upgrade Page diffuse method.

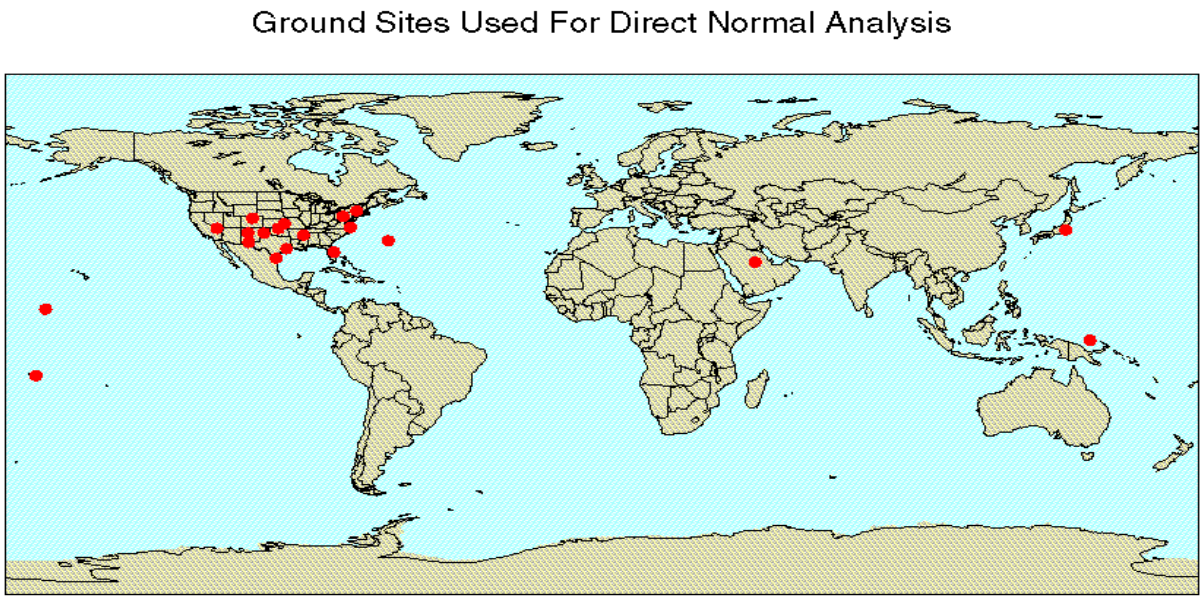

Figure 10. Sites with recent pyroheliometer and insolation data used for both diffuse and DNR comparisons.

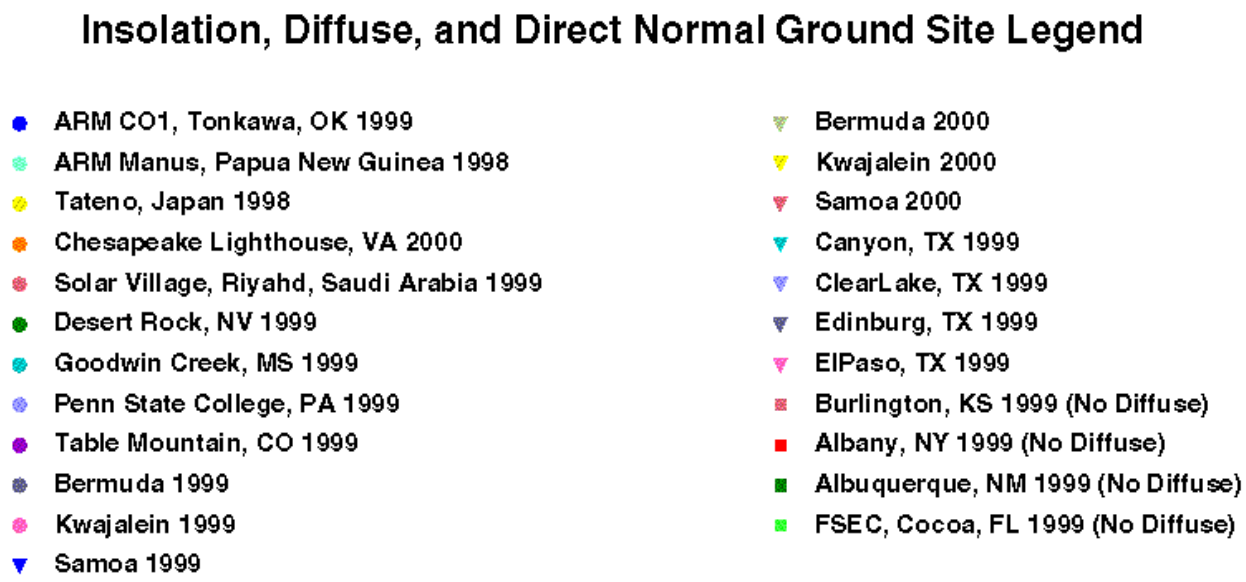

Figure 11. Color codes for sites used in both the diffuse and DNR comparisons that follow.

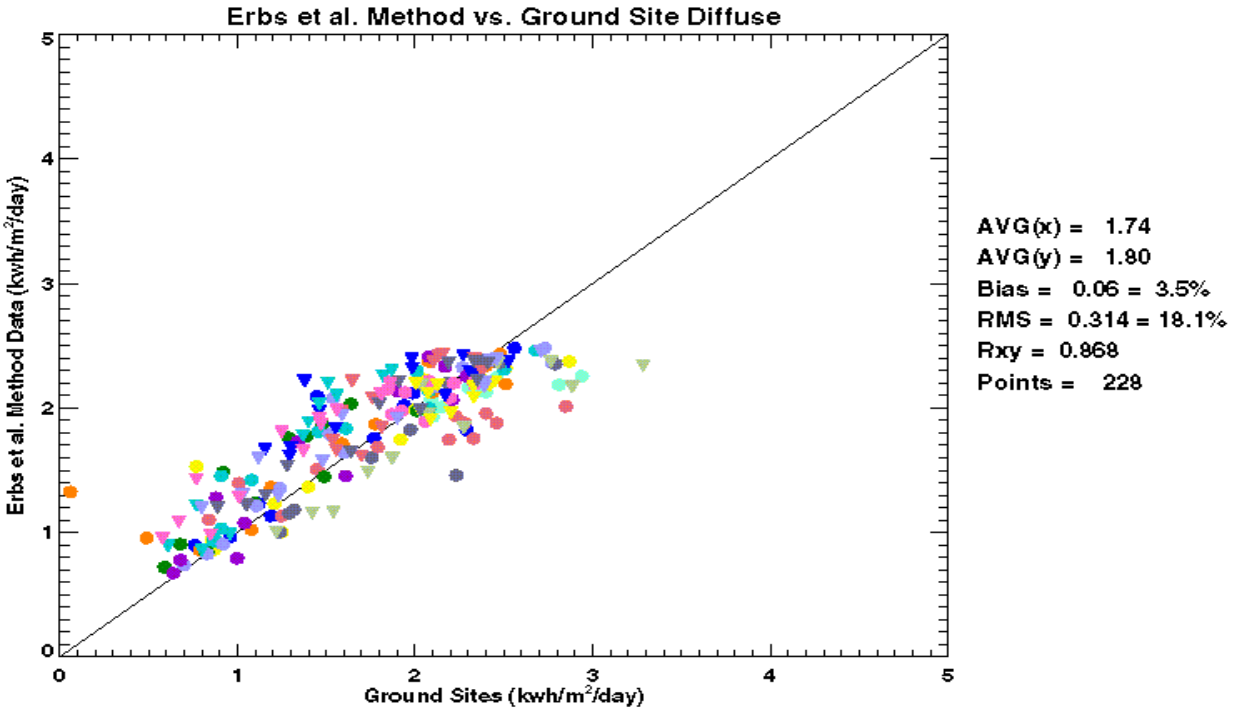

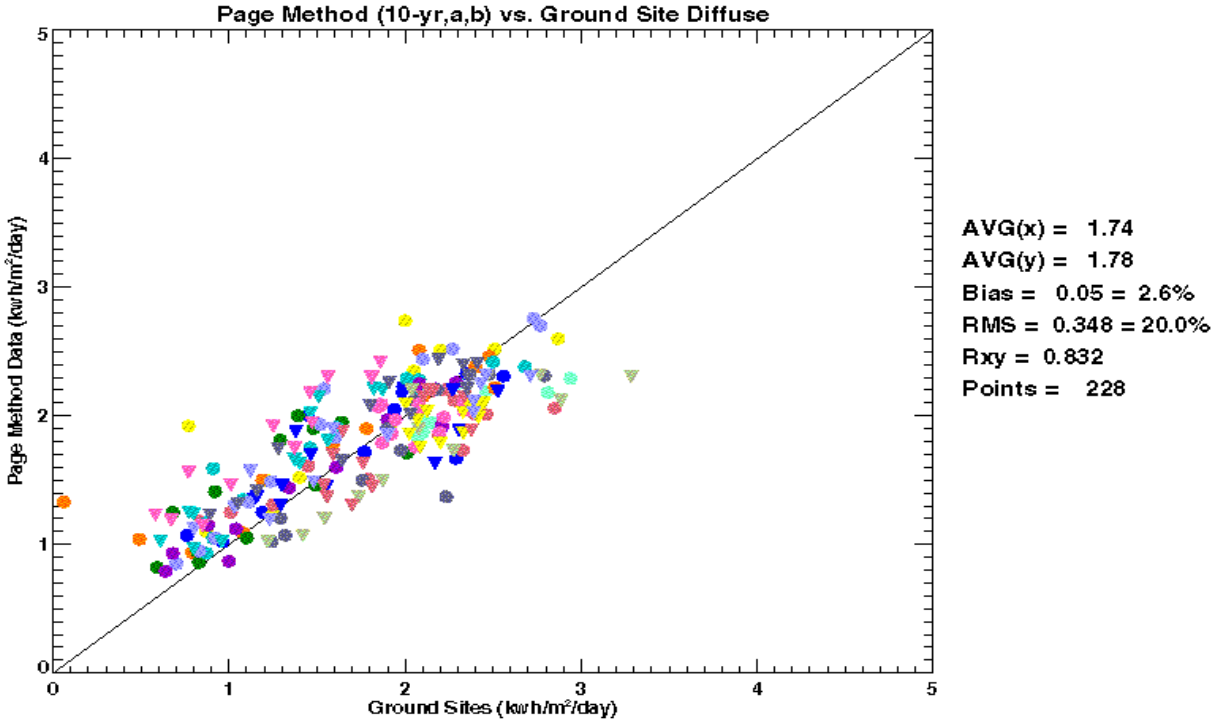

Figure 12. Statistical comparison of Erbs et al. method with ext ended Page 10-year method.

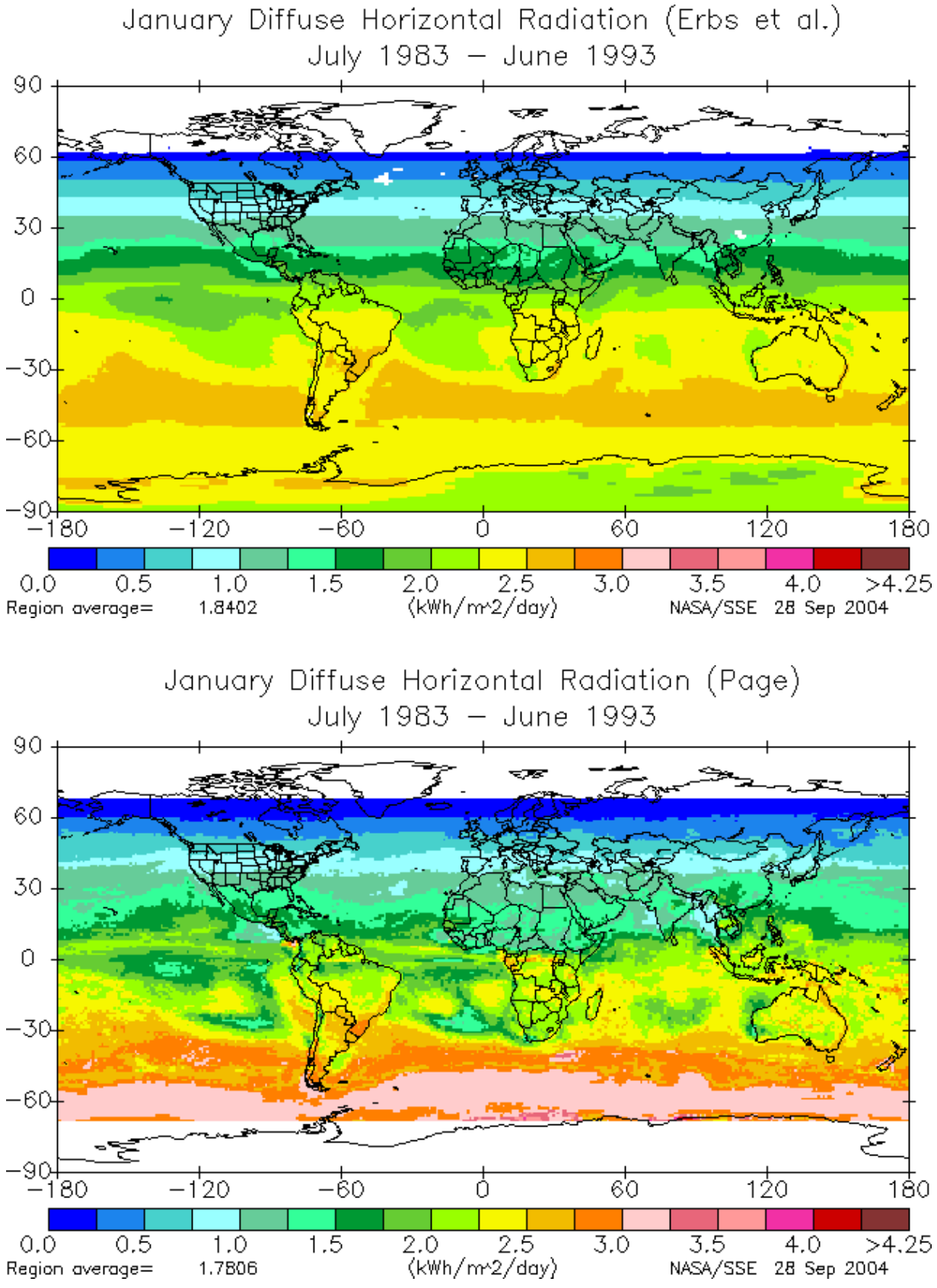

Figure 13. January global comparison of Erbs et al. method with extended Page 10-year method.

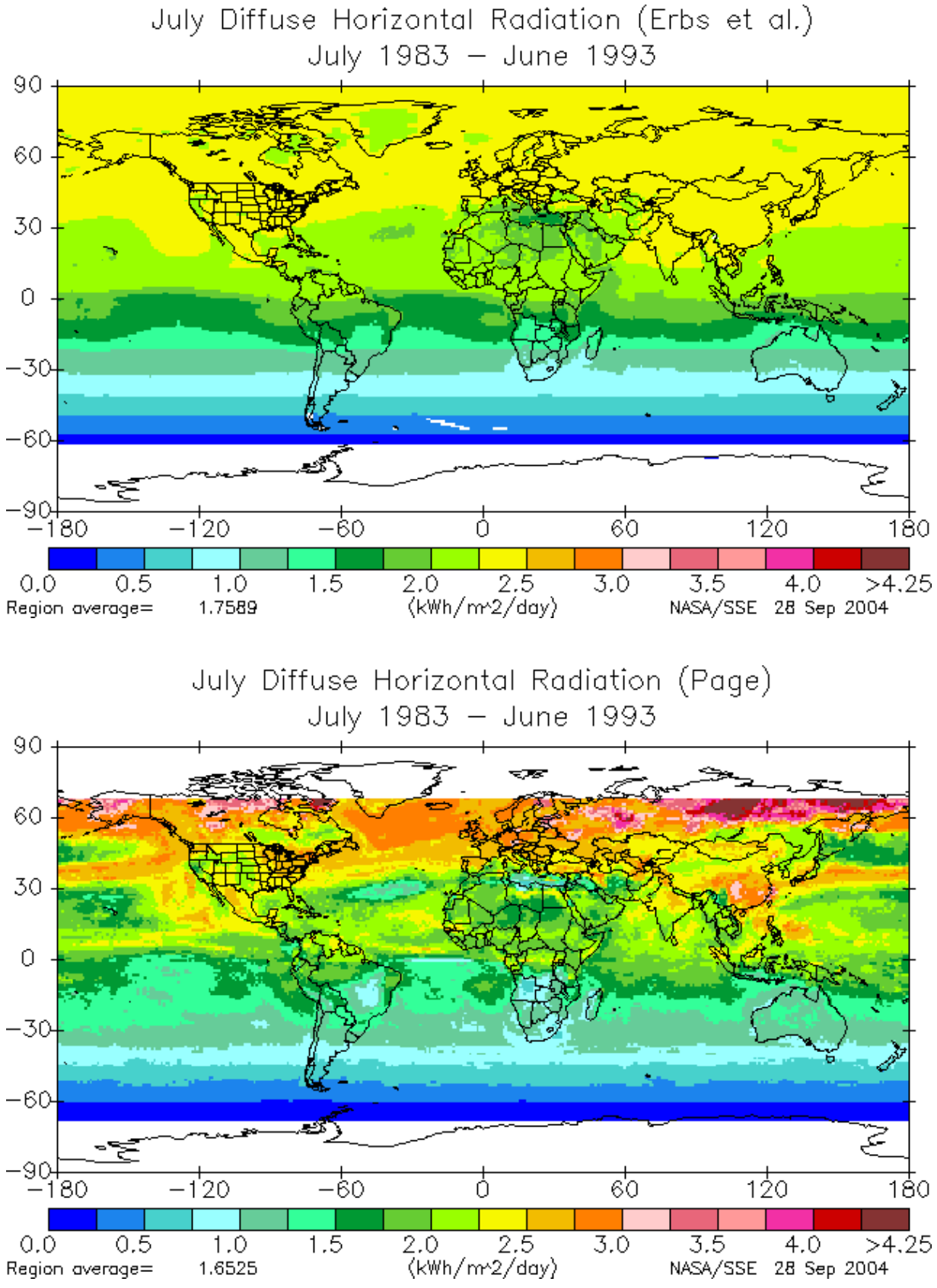

Figure 14. July global comparison of Erbs et al. method with extended Page 10-year method.

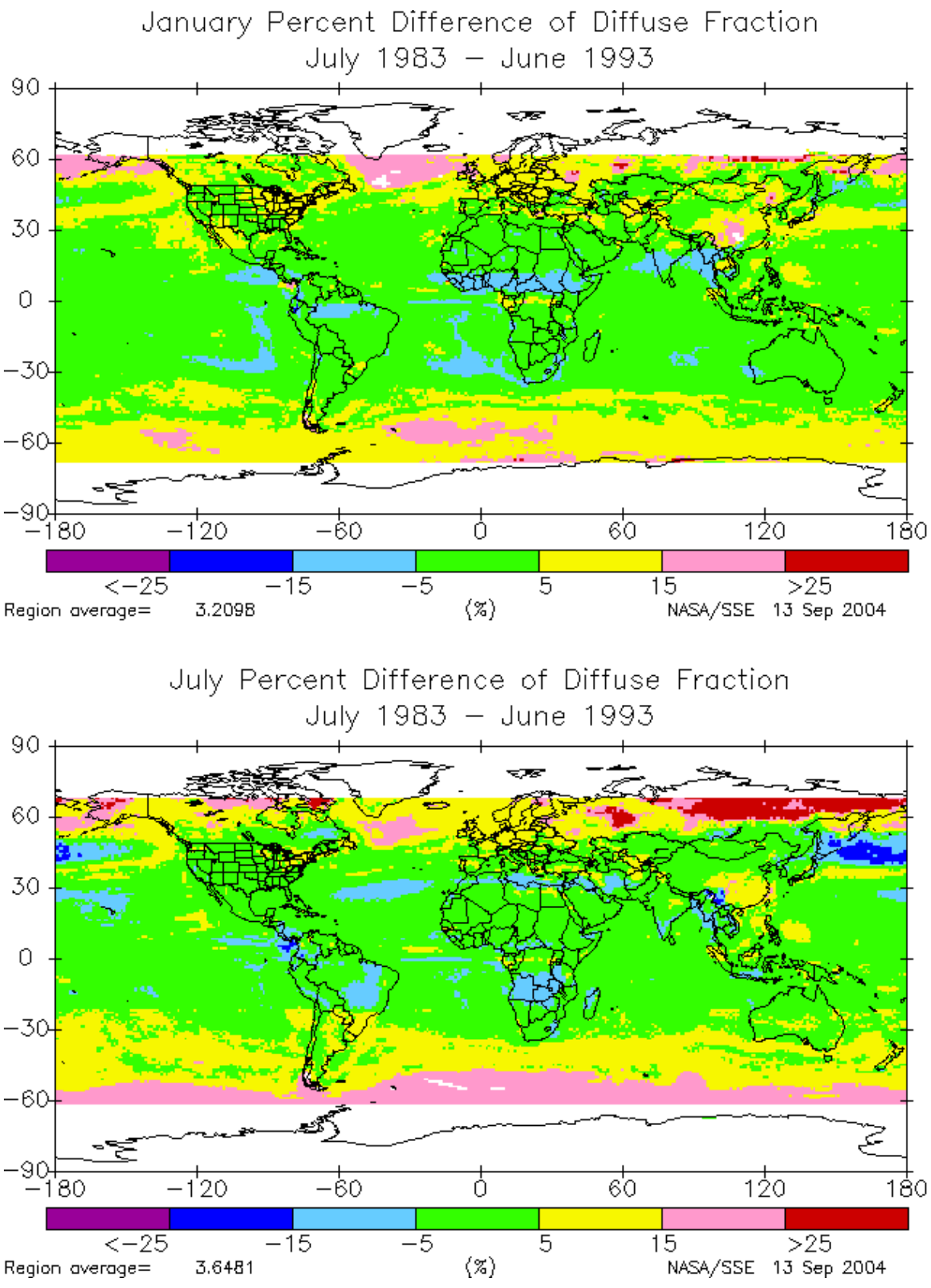

Figure 15. Differences between Erbs et al. and extended Page horizontal diffuse fraction, (Page H_d -Erbs et al. H_d)/H.

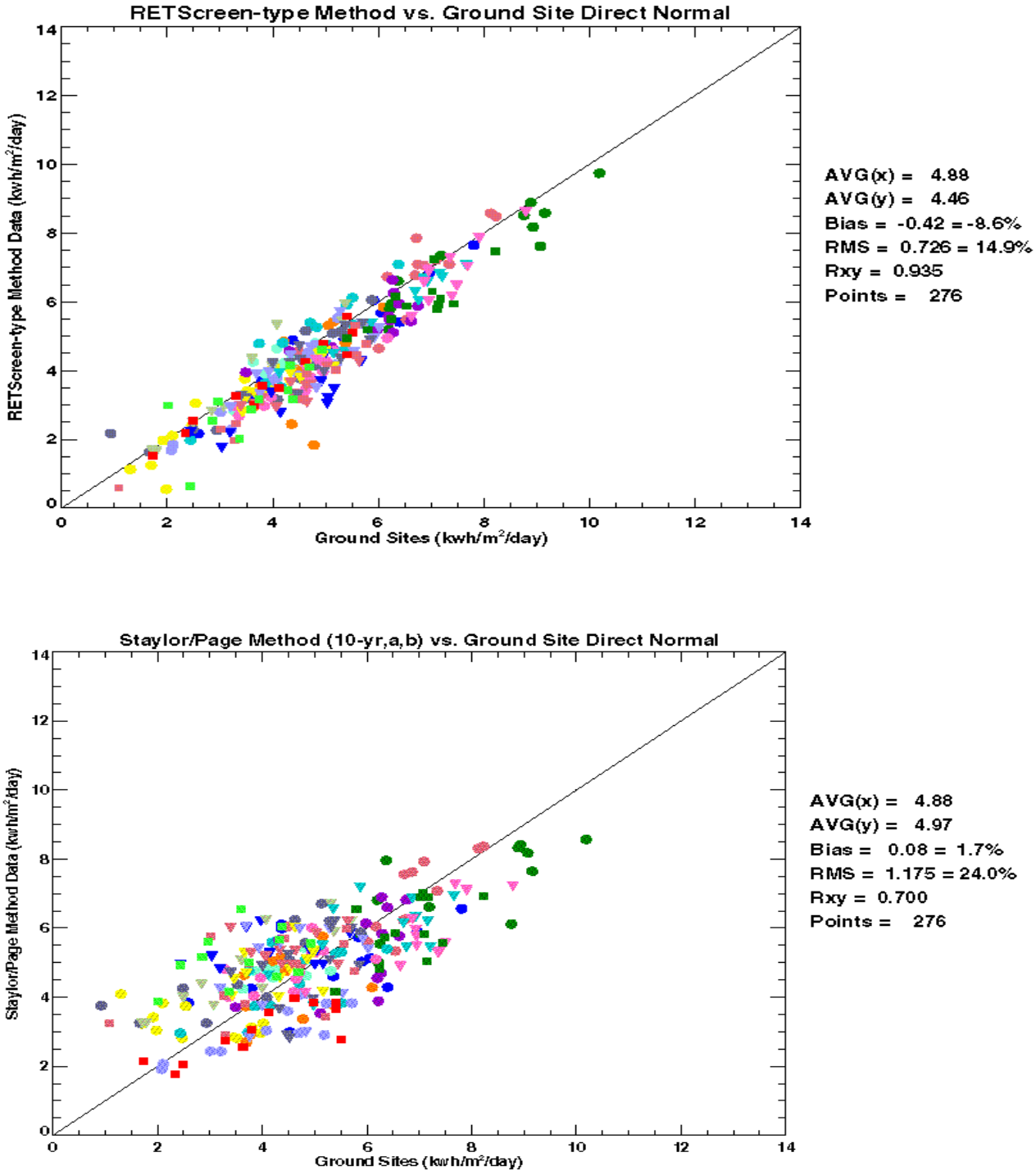

Figure 16. Statistical comparison of RETScreen-type method with extended Page 10-year method.

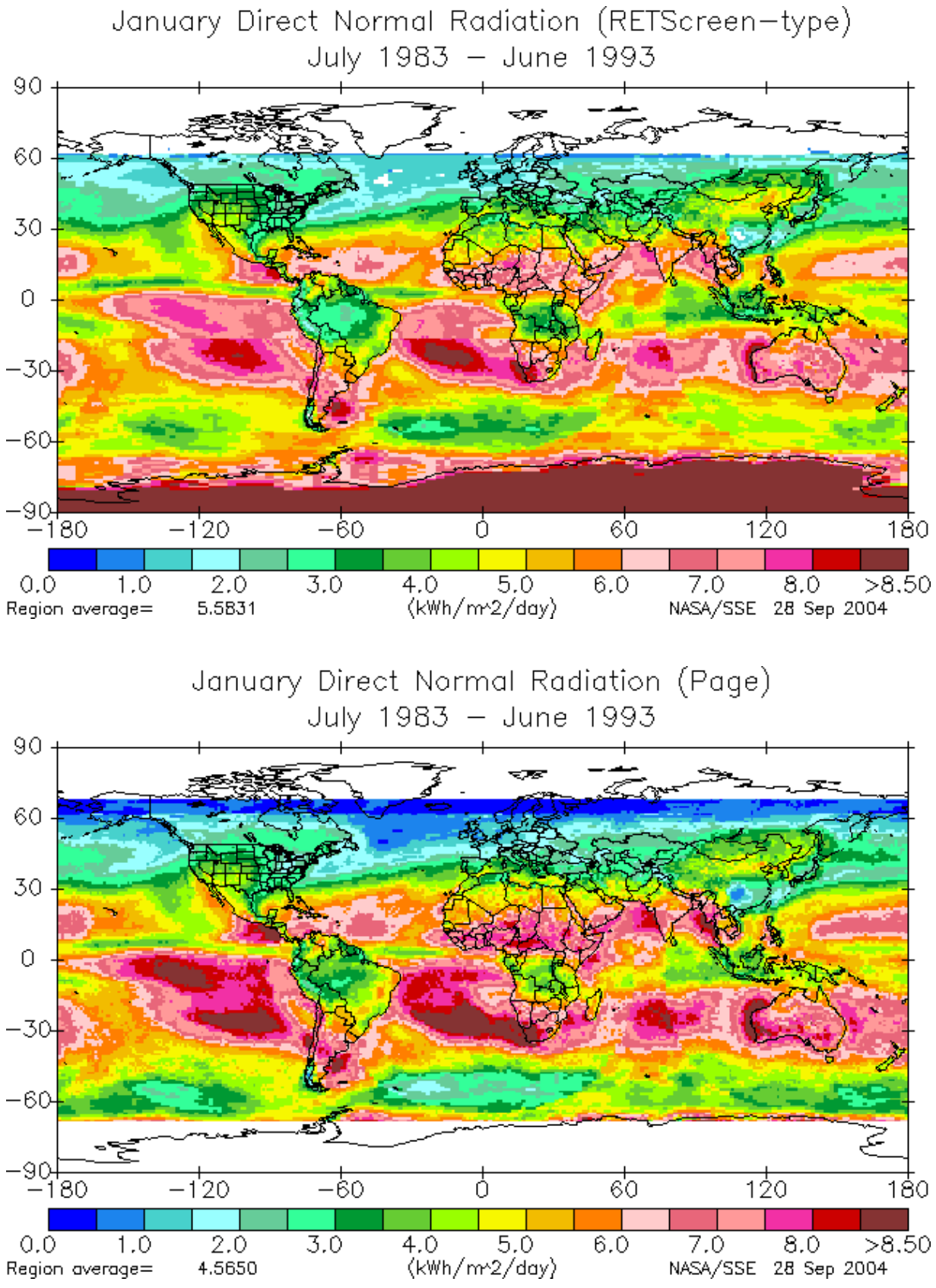

Figure 17. January global comparison of RETScreen-type method with extended Page method.

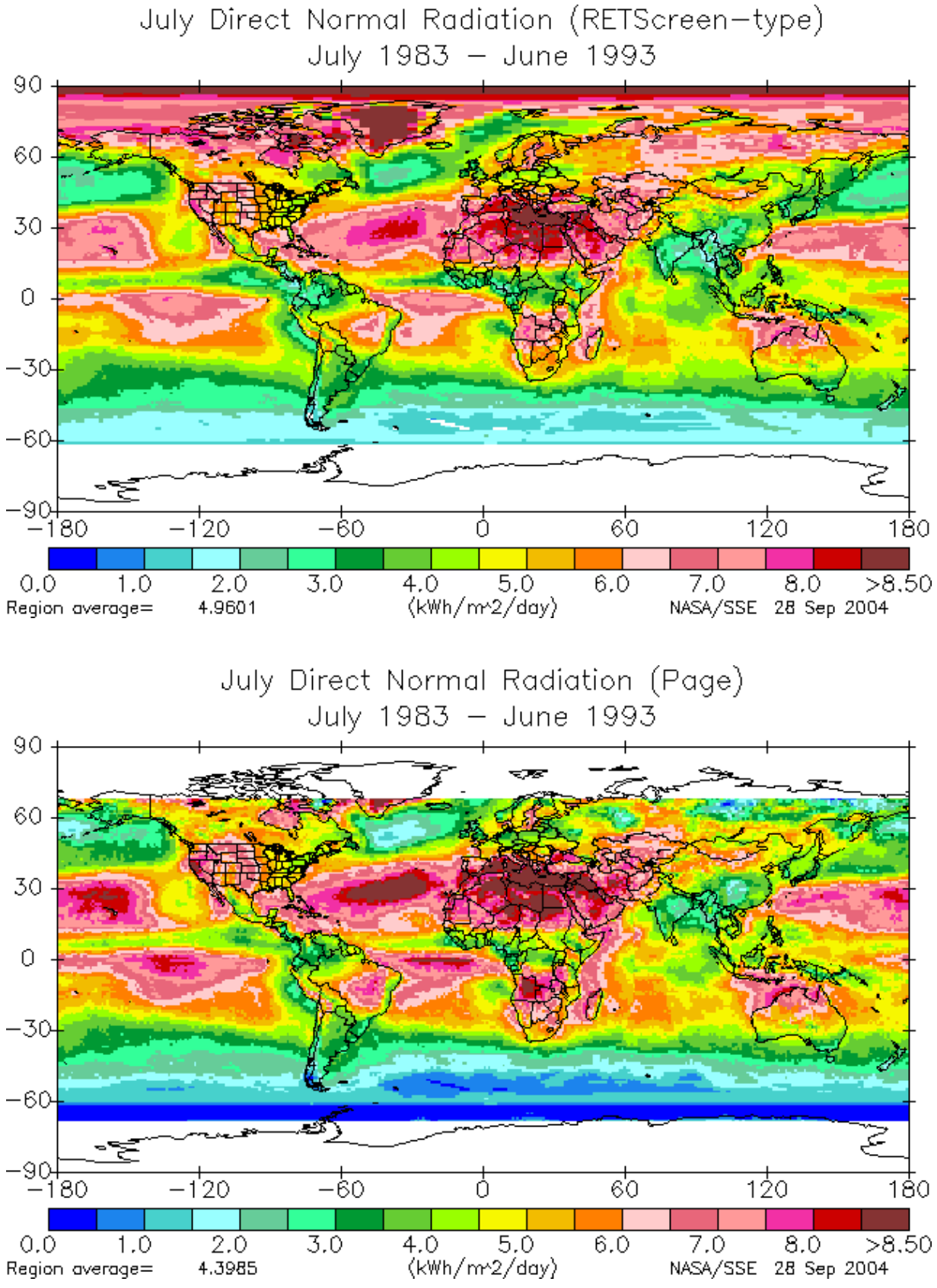

Figure 18. July global comparison of RETScreen-type method with extended Page method.

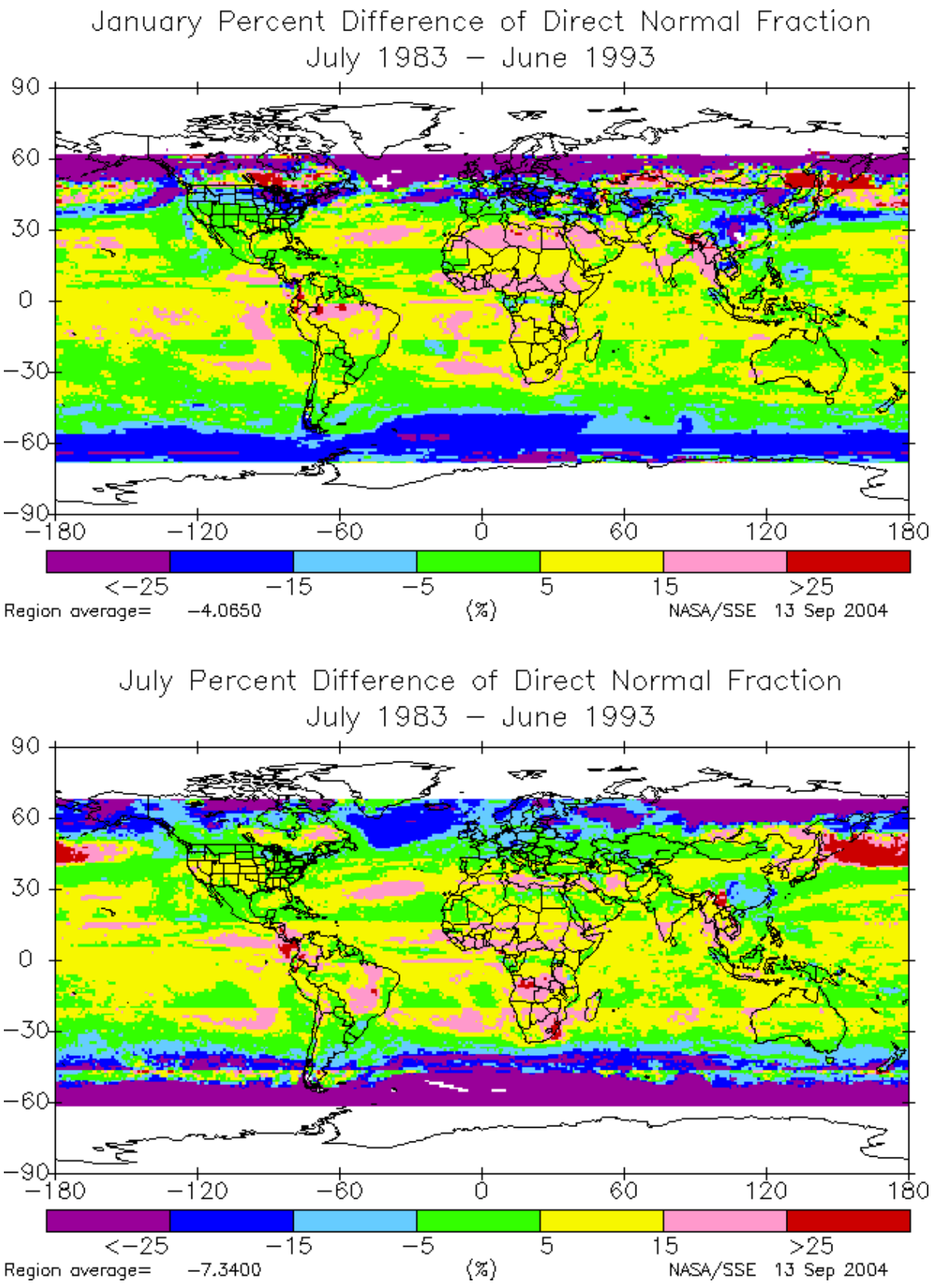

Figure 19. Differences between RETScreen-type and extended Page direct normal fraction, (Page DNR - RETS DNR)/H

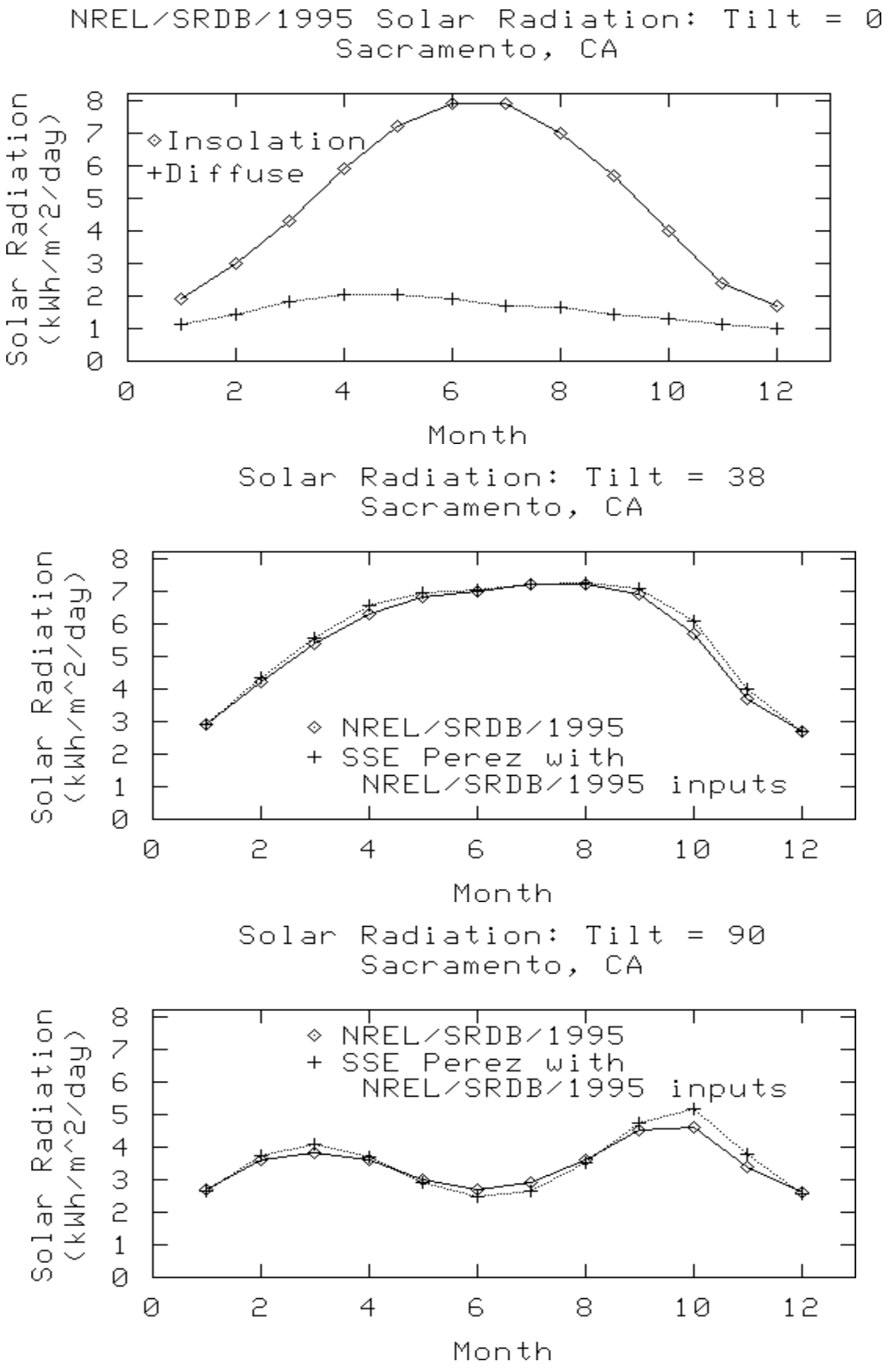

Figure 20. Comparison of SSE Perez tilt method with NREL Perez results.

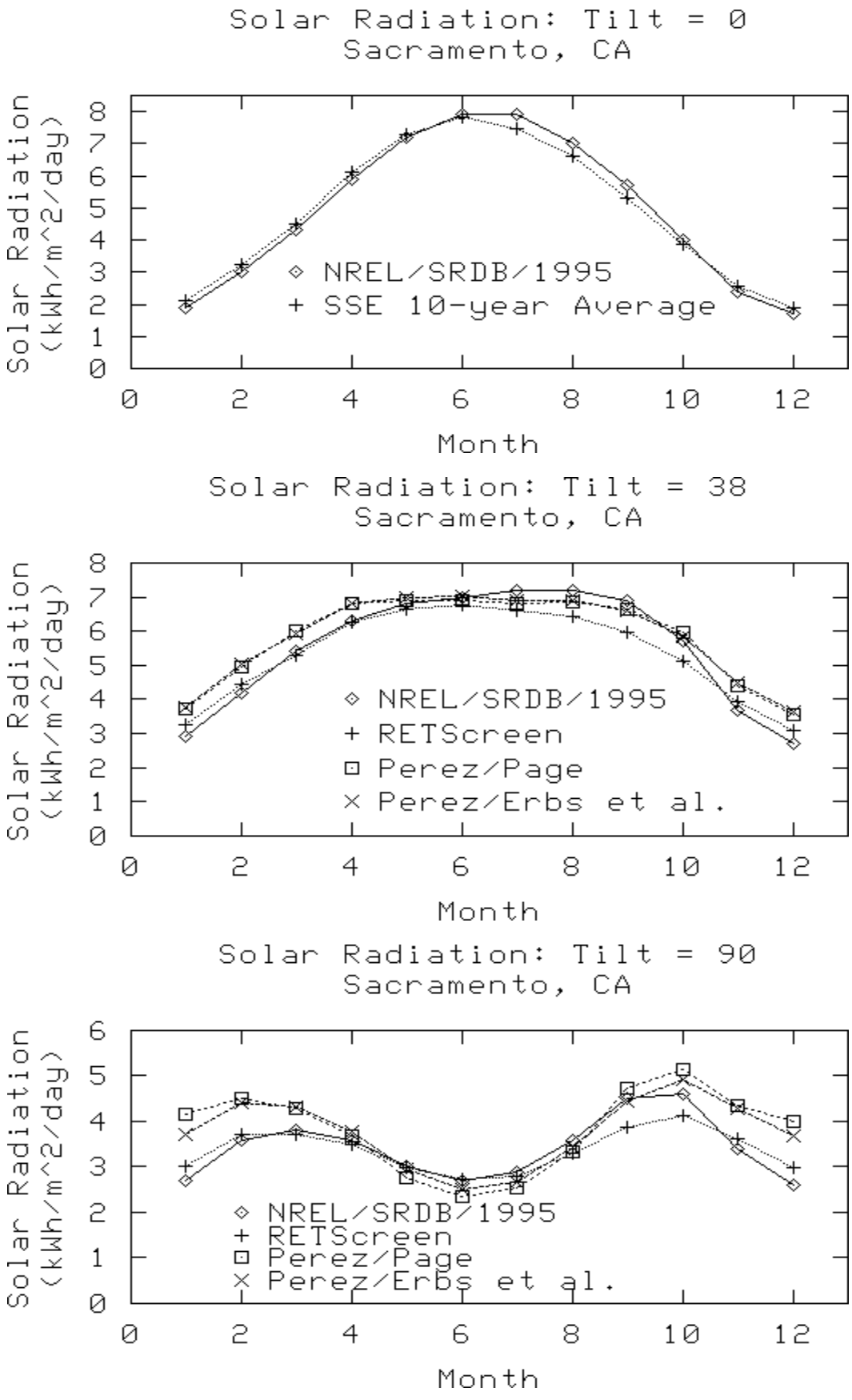

Figure 21. 10-year average tilt results for three SSE methods compared with NREL values.

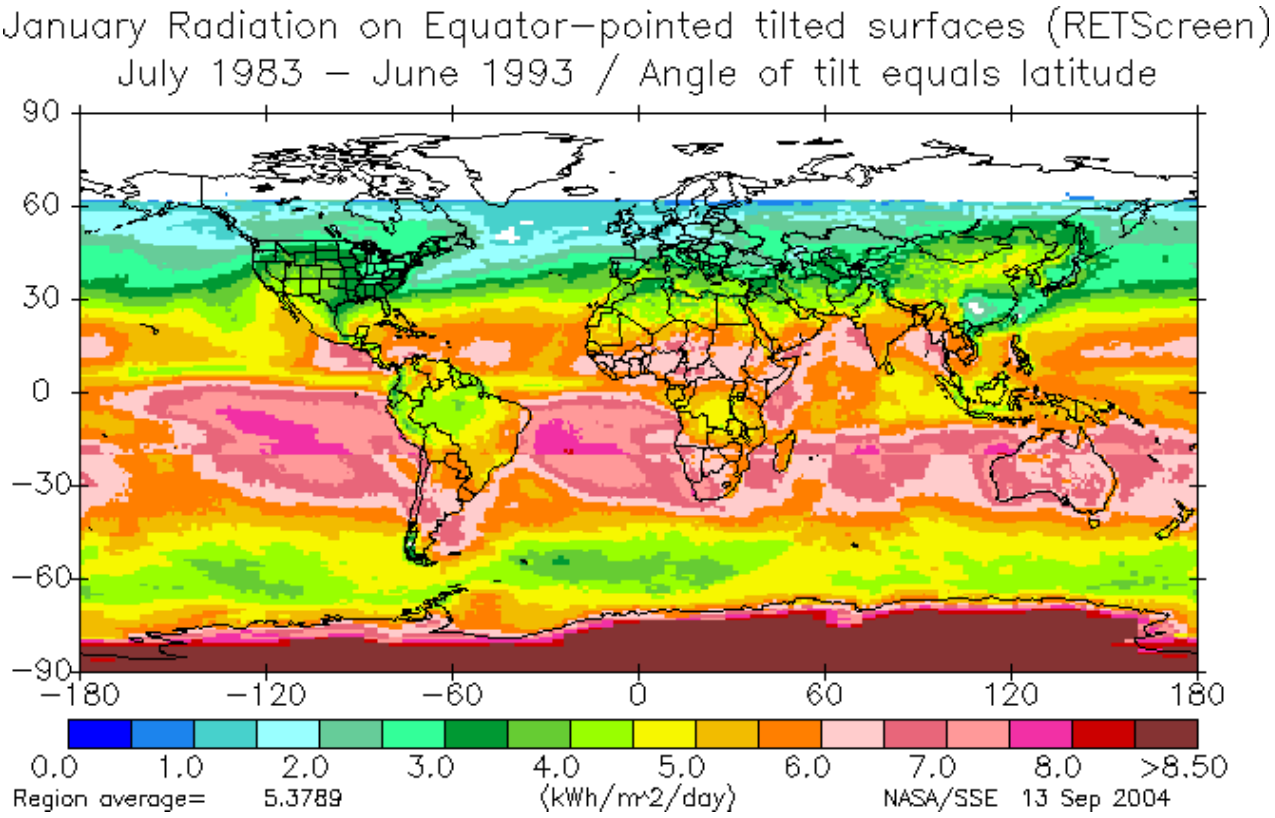

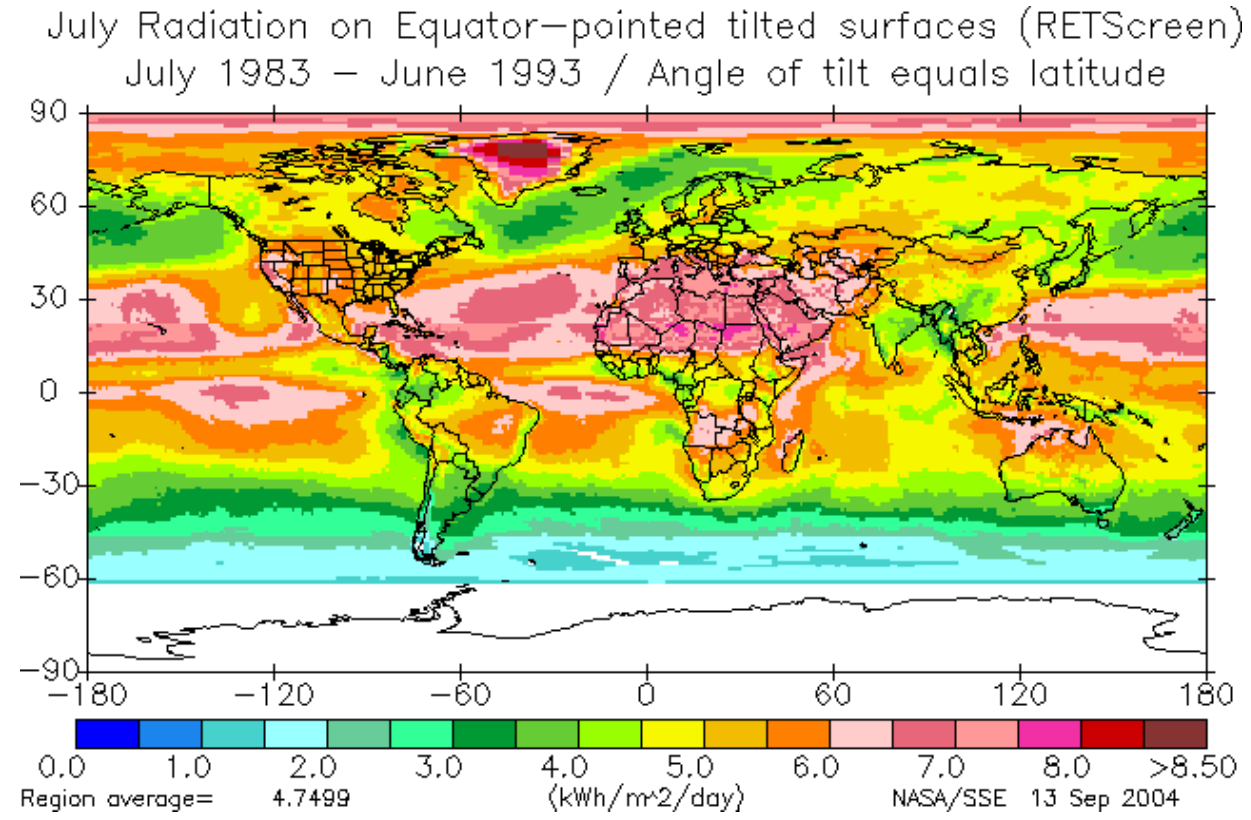

Figure 22. RETScreen method for solar radiation on equator-pointed panels tilted at latitude angles.

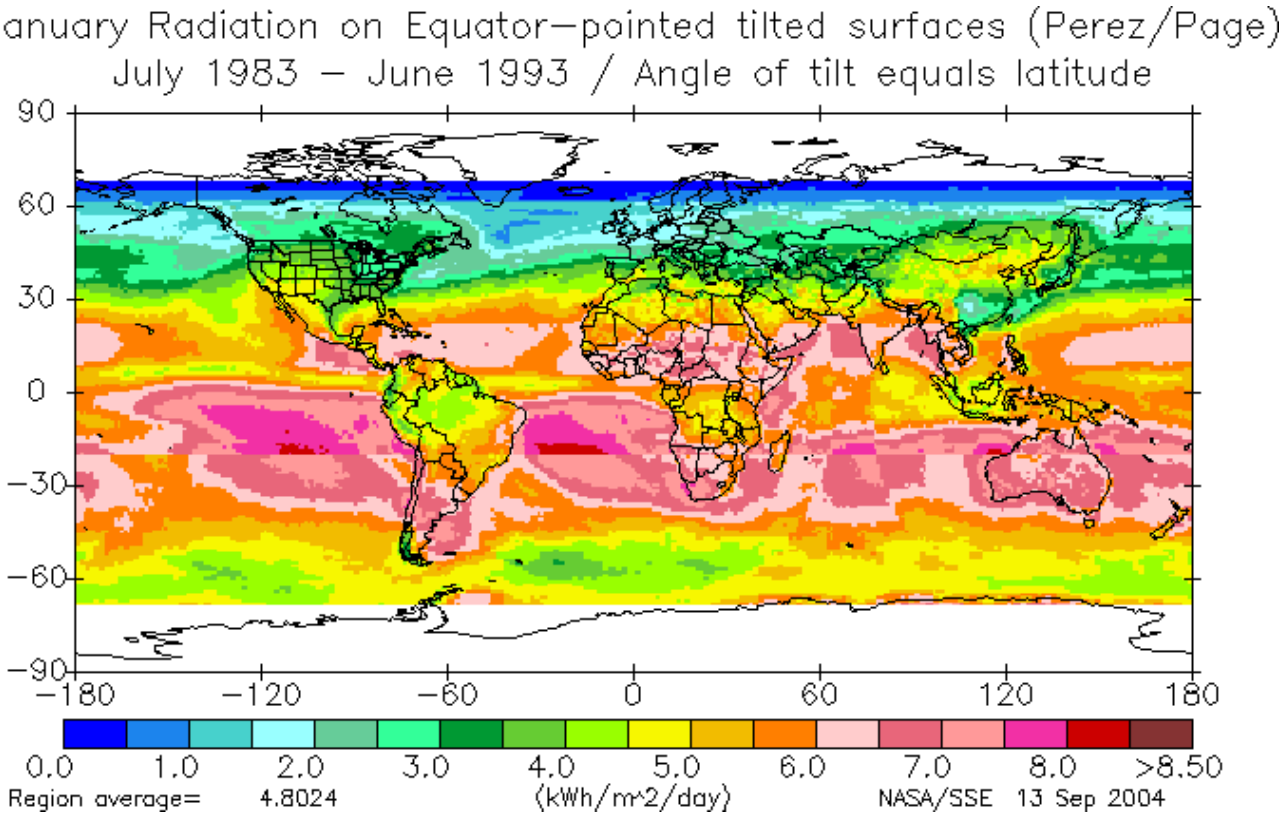

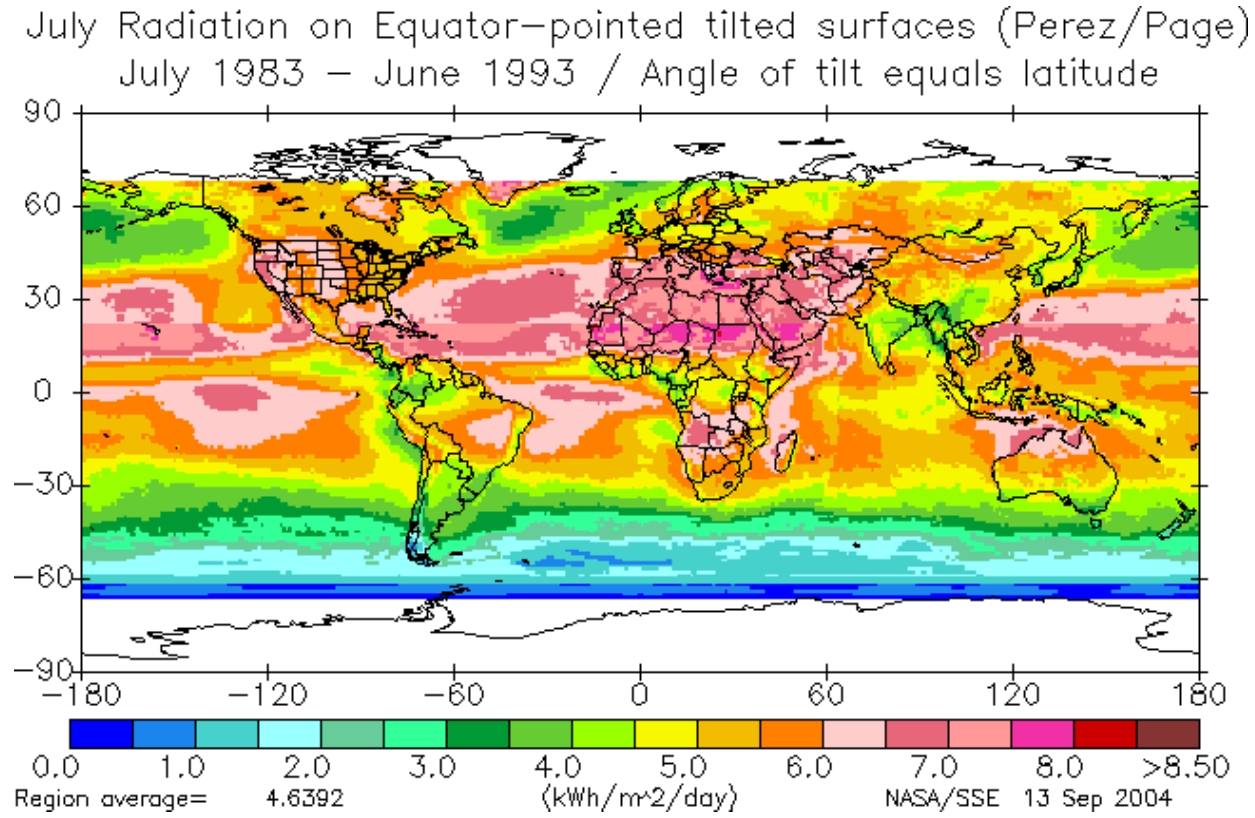

Figure 23. Perez/Page method for solar radiation on equator-pointed panels tilted at latitude angles.

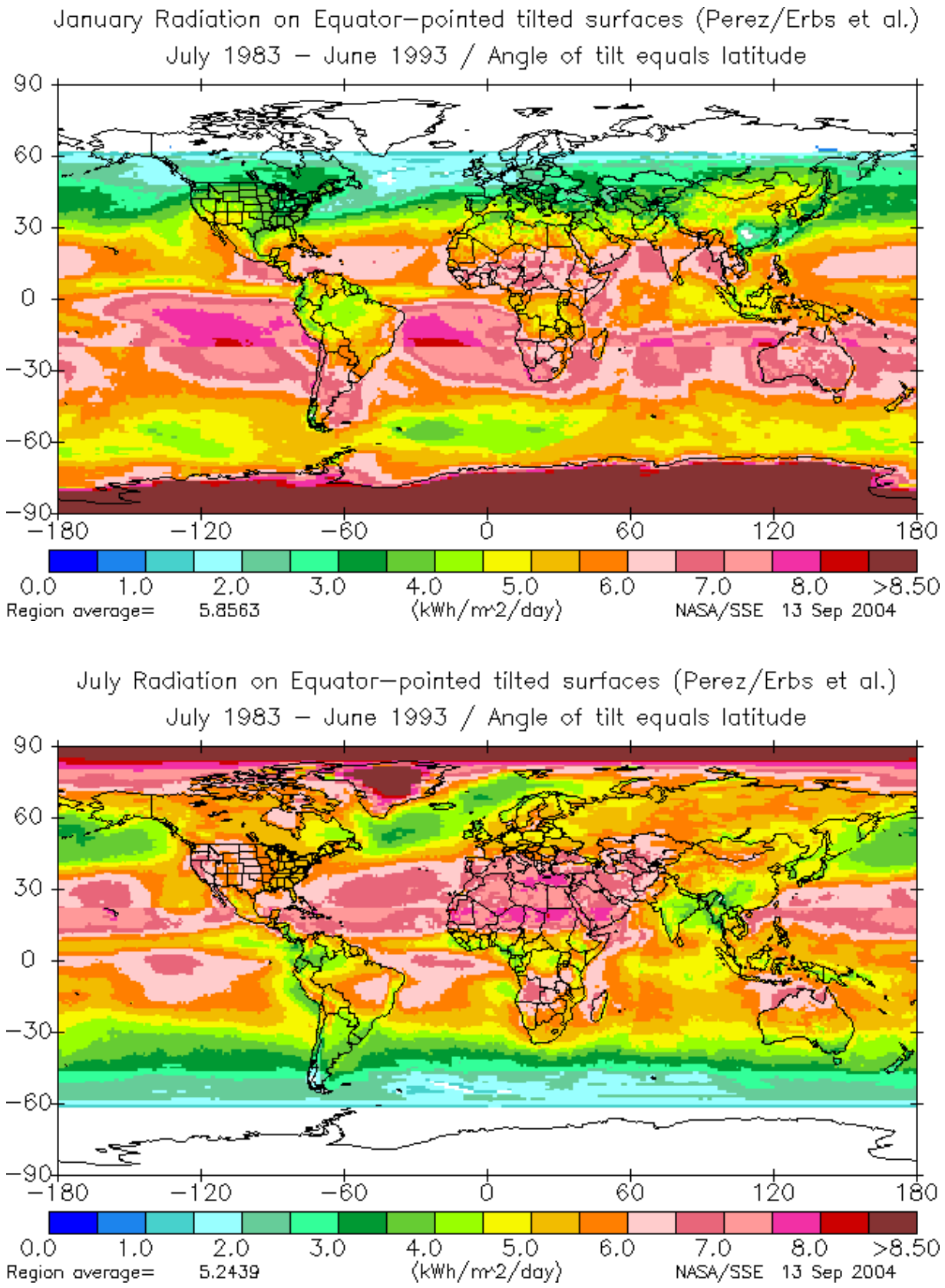

Figure 24. Perez/Erbs et al. method for solar radiation on equator-pointed panels tilted at latitude angles.

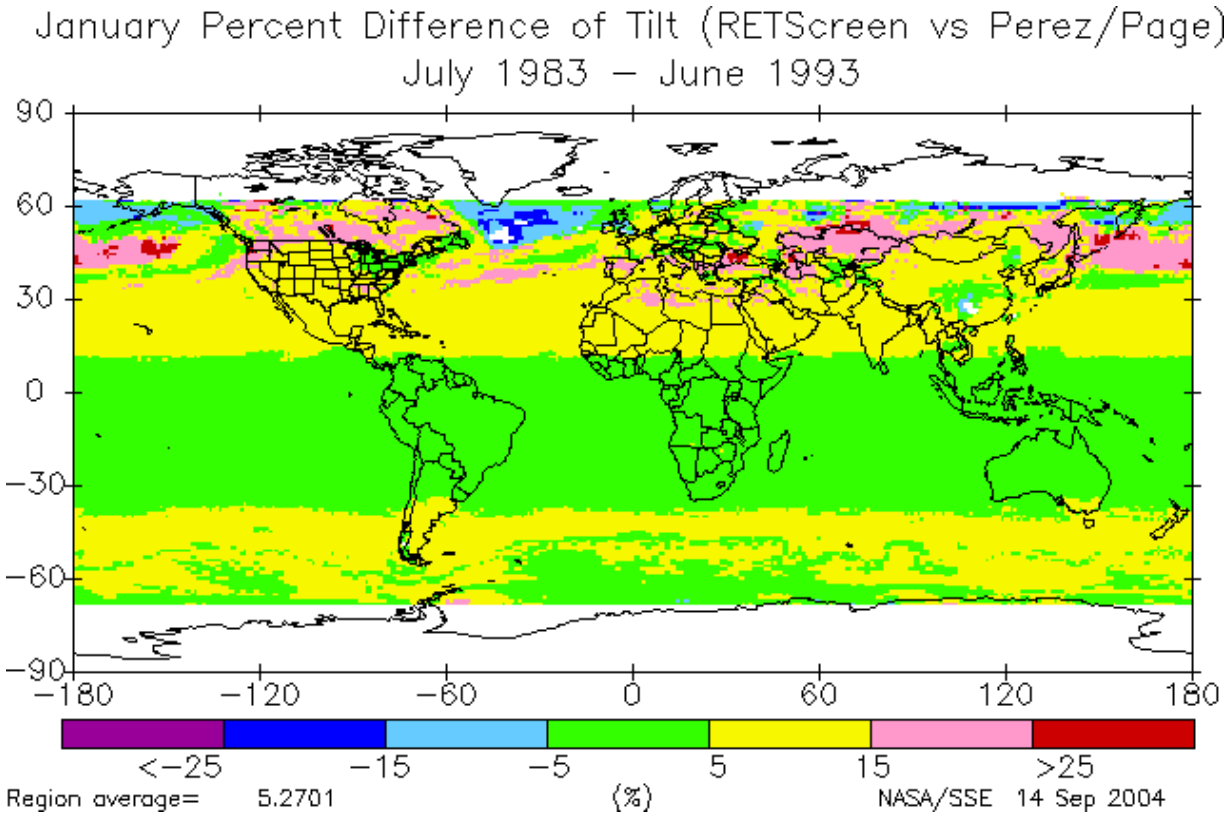

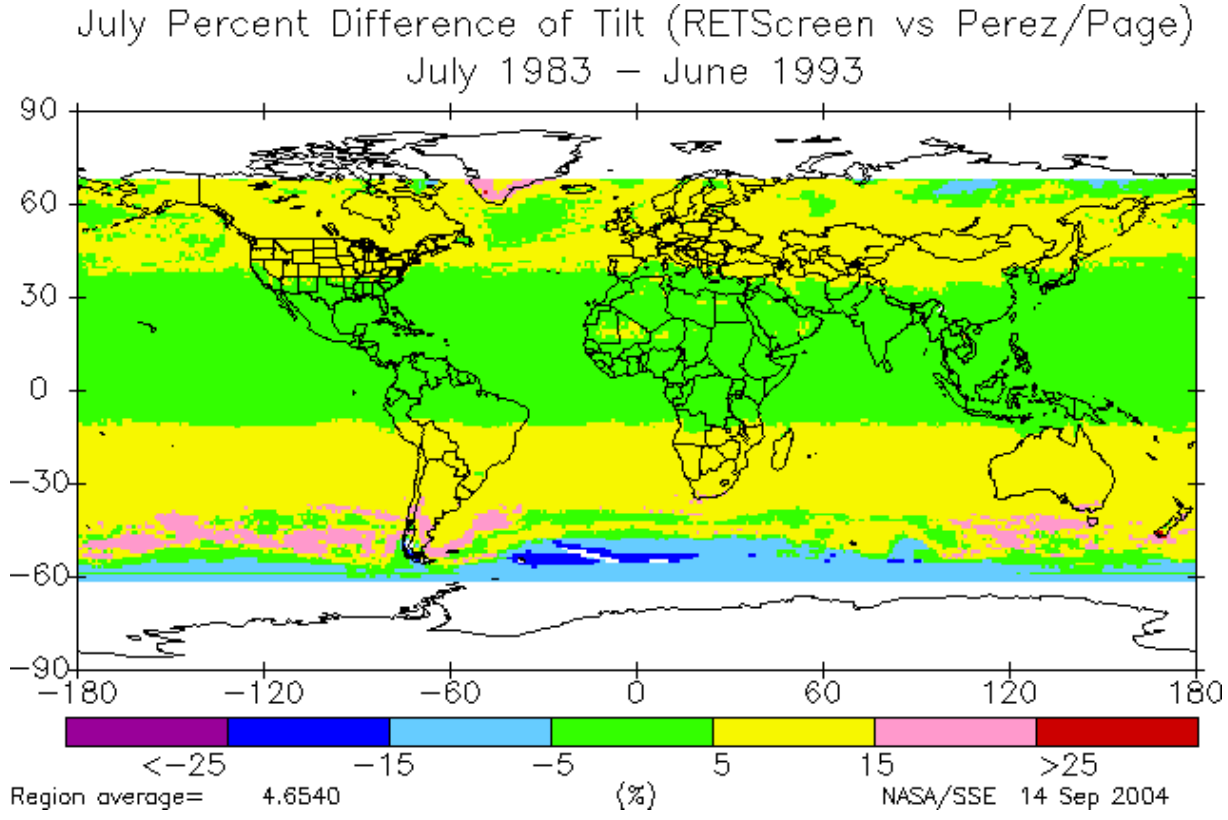

Figure 25. Differences between RETScreen and Perez/Page methods for solar radiation on equator-pointed panels tilted at latitude angles, (Perez/Page Tilt - RETS Tilt)/RETS Tilt.

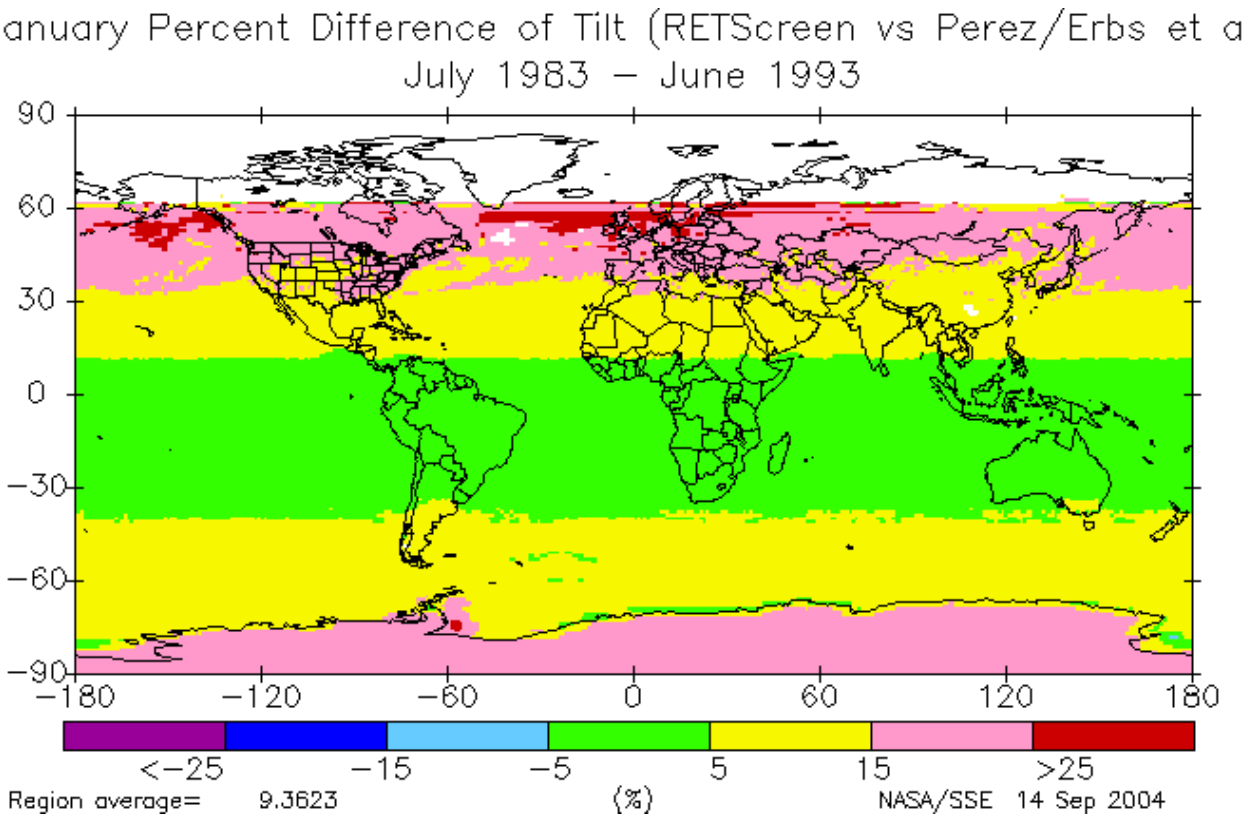

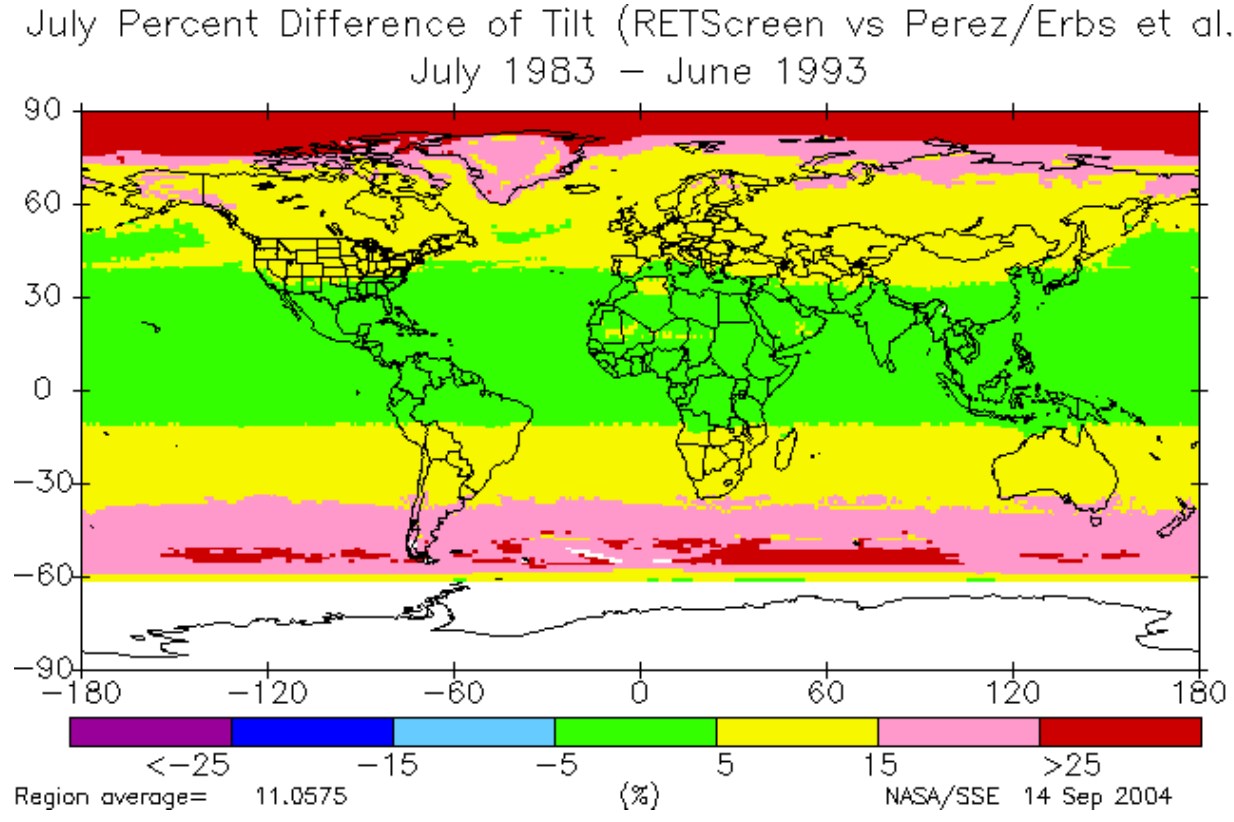

Figure 26. Differences between RETScreen and Perez/Erbs et al. methods for solar radiation on equator-pointed panels tilted at latitude angles, (Perez/Erbs et al. Tilt - RETS Tilt)/RETS Tilt.

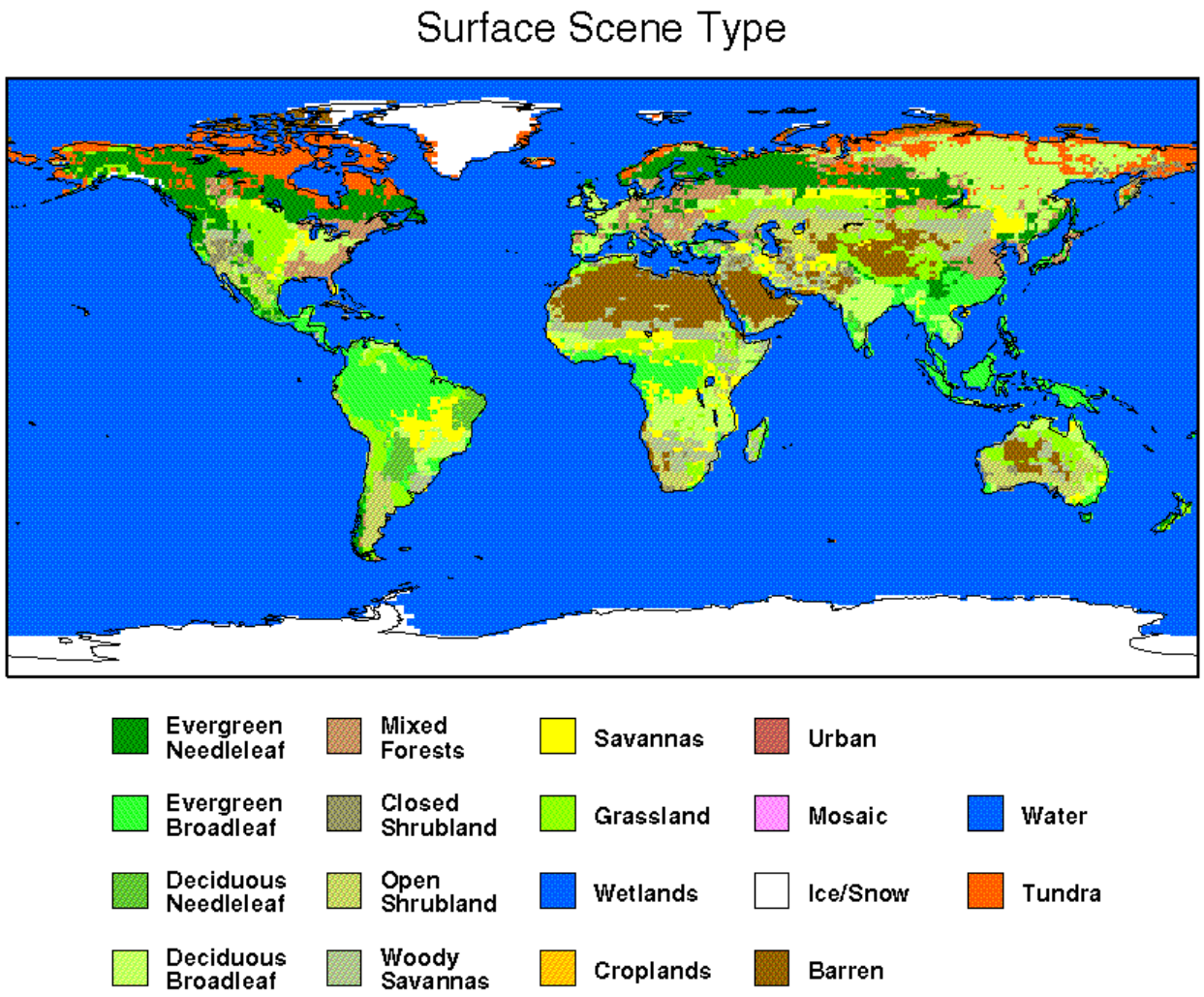

Figure 27. International Geosphere and Biosphere Project (IGBP) scene types.

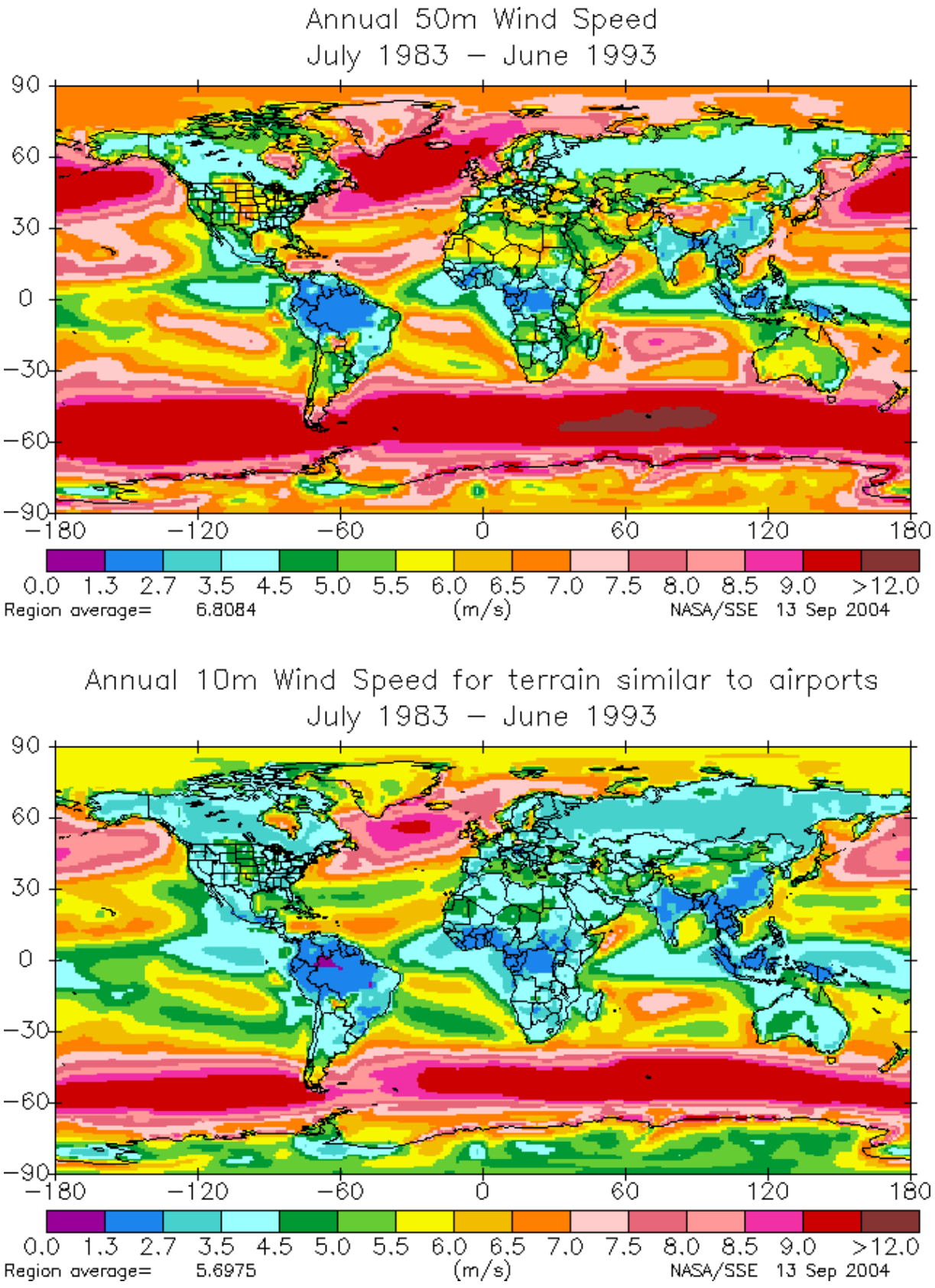

Figure 28. SSE estimates of wind velocity at 50 and 10m above the ground, water, or snow/ice surface.

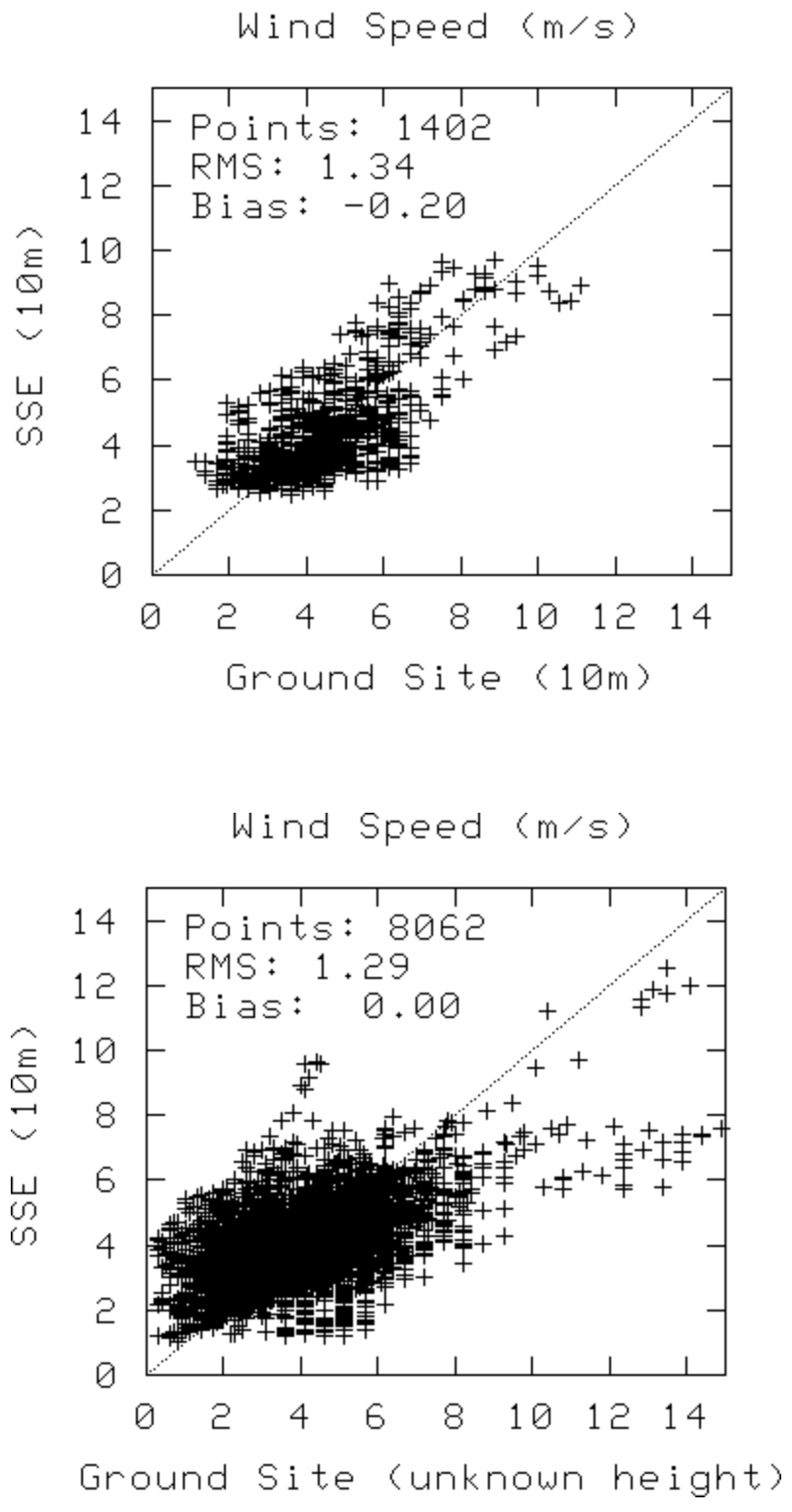

Figure 29. Comparison of 10-year Release 4 SSE 10-m wind speed with 30-year RETScreen site data.

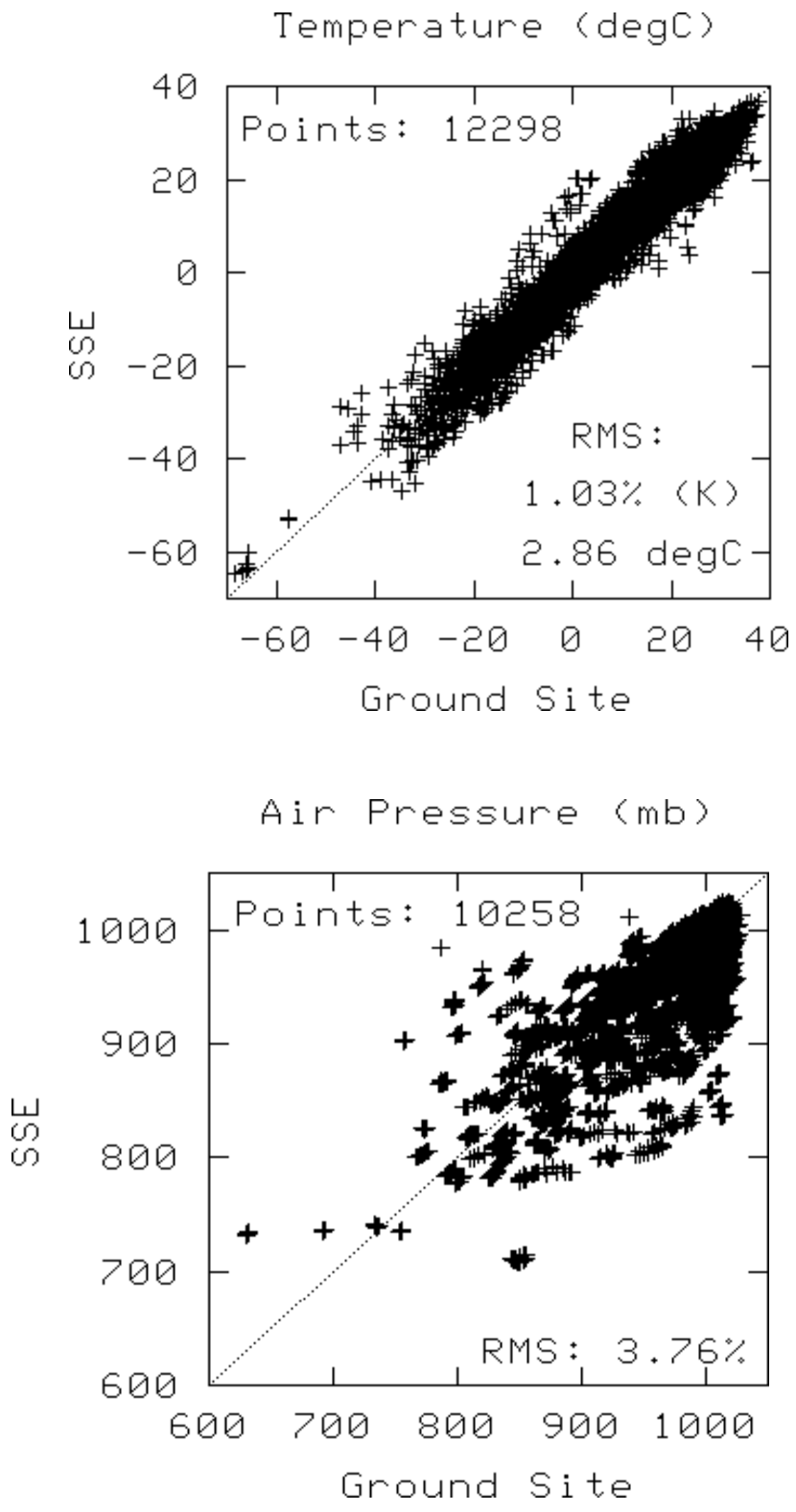

Figure 30. Comparison of 10-year SSE 10-m temperature and pressure with 30-year RETScreen site data.

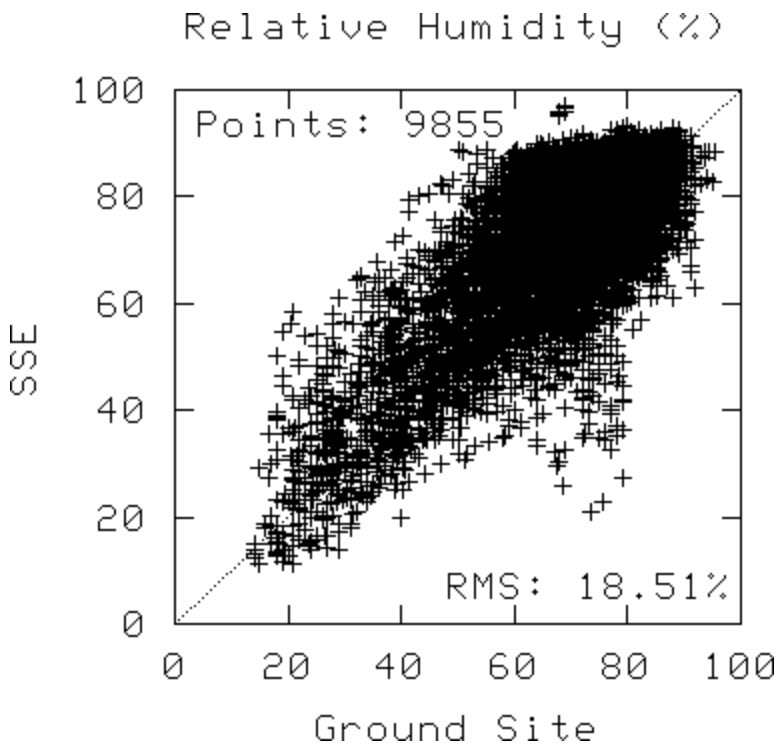

Figure 31. Comparison of 10-year SSE 10-m relative humidity with 30-year RETScreen site data.